sid.inpe.br/mtc-m21c/2020/12.21.15.24-RPQ

WATER COOLED TOROIDAL FIELD COIL. FORCED CONVECTION TURBULENT FLOW REGIME

Gerson Otto Ludwig

URL do documento original:
<http://urlib.net/8JMKD3MGP3W34R/43QQMPB>

INPE
São José dos Campos
2020

PUBLICADO POR:

Instituto Nacional de Pesquisas Espaciais - INPE
Coordenação de Ensino, Pesquisa e Extensão (COEPE)
Divisão de Biblioteca (DIBIB)
CEP 12.227-010
São José dos Campos - SP - Brasil
Tel.:(012) 3208-6923/7348
E-mail: pubtc@inpe.br

sid.inpe.br/mtc-m21c/2020/12.21.15.24-RPQ

WATER COOLED TOROIDAL FIELD COIL. FORCED CONVECTION TURBULENT FLOW REGIME

Gerson Otto Ludwig

URL do documento original:
<http://urlib.net/8JMKD3MGP3W34R/43QQMPB>

INPE
São José dos Campos
2020

Water cooled toroidal field coil
Forced convection turbulent flow regime

G.O. Ludwig[1,2] *E-mail address:* gerson.ludwig@inpe.br
[1]National Institute for Space Research, 12227-010 São José dos Campos, SP, Brazil
[2]National Commission for Nuclear Energy, 22294-900 Rio de Janeiro, RJ, Brazil
(Dated: 30 May 2020)

A one-dimensional pipe flow model is used to address the steady-state cooling requirements for the toroidal field copper coil of a compact tokamak. The report focuses on the forced convection turbulent flow regime in the liquid phase, which may extend to the superheated regime of the coolant. The largest values of the toroidal magnetic field that can be attained within reasonable limits of temperature rise, pressure drop and pumping power are considered.

I. INTRODUCTION

There has been considerable interest in compact, usually low-power, tokamak reactors for quite some time [1–8]. Compact tokamaks have been considered as an alternative route for the commercial viability of nuclear fusion [1, 2, 7, 8], besides allowing the early use of fusion neutrons [3, 5, 6]. Spherical tokamaks with increased magnetic field seem to be a suitable choice for these applications. Moreover, a main purpose in developing low-power reactors is to reduce the first-wall load to levels that can be handled with currently available technologies [4]. Clearly, it is important to assess the technological limits in the development of compact reactors; in particular, the largest toroidal magnetic field values that can be reasonably attained.

The required toroidal magnetic field can be obtained using a replaceable copper center post [1, 3, 6]. However, the cooling of the central column puts great limitations in the design of the toroidal field coil (TF coil). The heat removal from the center post must be balanced with the spacing constraints and the admissible mechanical stress limit, for a given value of the magnetic induction at the plasma center. This will be eased only with the use of high-temperature superconductors, still a technological challenge [8], although low-temperature superconducting TF coils have also been considered [2, 7].

This report examines the forced water cooling of the TF coil for a compact tokamak using a simple one-dimensional pipe flow model. In general, the simulation of flow and heat transfer along a cooling channel requires a computationally expensive tridimensional representation. However, the ratio of length over diameter in the TF system is large; and the flow inside each cooling channel can be considered fully developed. This allows using one-dimensional pipe flow equations, greatly increasing the computational efficiency. The problem can be further simplified introducing an effective transverse distance for heat conduction out off the copper. This effective distance defines in a simple way the boundary layer heat transfer conditions on the tube wall.

Section II presents the simplified central column and TF coil geometry of a small, compact tokamak. Section III concerns the cooling requirements for a TF coil producing a central magnetic field in the range $1.0 \sim 3.0\,\mathrm{T}$. Conclusions and comments are given in Section IV. Appendix A reviews some correlations of the convective heat-transfer coefficient and friction factor for water in turbulent flow. The thermophysical properties of water are listed in the Appendix B. A few geometric configurations for the center post cooling channels are presented in the Appendix C.

II. SIMPLIFIED TOROIDAL FIELD COIL GEOMETRY

This section presents the basic parameters of a compact tokamak focusing on the center post geometrical constraints. A preliminary design is made of the center post of a TF copper magnet for a small device with major radius $R_0 = 0.5\,\mathrm{m}$ and minor radius $a = 0.3\,\mathrm{m}$ (the plasma aspect ratio is $A = R_0/a = 1.667$). The plasma shape definition is completed with the elongation $\kappa = 2.0$ and the triangularity $\delta = 0.4$.

The plasma shape is used merely to set the size of the device. The schematic figures displayed in this section include simplified cross-sectional views of the plasma, vacuum vessel and TF coil. They are used to examine the spacing between the main components of the tokamak in the central region. The main geometrical parameters of the tokamak, and the TF coil in particular, are either defined or evaluated in this section. The final choice of dimensions depends mostly on the divertor configuration, not yet defined. Two basic configurations for the central post are presented: a small diameter center post with sufficient clearance for either a thin inboard shield or a transformer solenoid; and a relatively large diameter center post with vanishing clearance between the TF coil and the vacuum vessel.

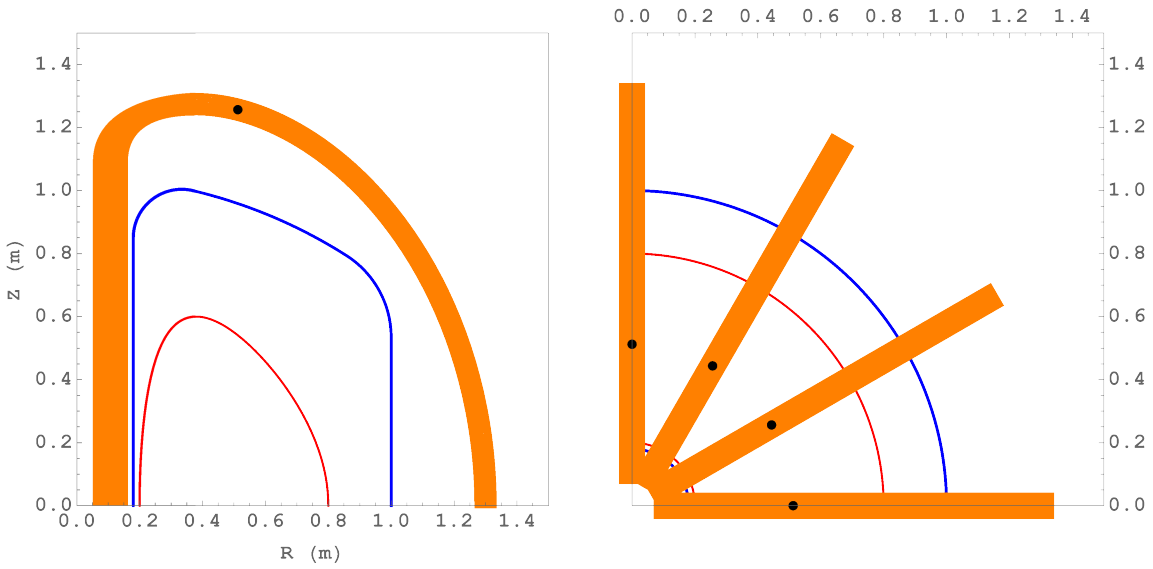

FIG. 1. Schematic representations of the TF coil (elastic line with variable width), simplified vacuum vessel centerline and enclosed plasma boundary: the left and right-hand pictures show the poloidal and equatorial cross-sections, respectively. The points on each turn of the TF coil indicate the half-length positions along the centerline.

The plasma boundary is defined by the parametric equations

$$\begin{aligned} R(\theta) &= R_0 + a\left(\cos\theta - \frac{1}{2}C_\delta \sin^2\theta\right), \\ Z(\theta) &= aC_\kappa\left(1 - \frac{1}{2}C_\delta\cos\theta\right)\sin\theta, \end{aligned} \tag{1}$$

where C_δ and C_κ are the coefficients of triangularity and elongation, respectively, given in terms of the triangularity δ and elongation κ by

$$\begin{aligned} C_\delta &= \frac{8}{3}\delta - 4\sqrt{2+\frac{4}{9}\delta^2}\,\sin\left[\frac{1}{3}\arctan\left(\frac{\sqrt{3}\,(135-16\delta^2)\,\delta}{27\sqrt{96-11\delta^2+32\delta^4}}\right)\right] = 0.4244, \\ C_\kappa &= \kappa\left(\frac{8C_\delta}{\left(3+\sqrt{1+2C_\delta^2}\right)\sqrt{2\sqrt{1+2C_\delta^2}-2+2C_\delta^2}}\right) = 1.9581. \end{aligned} \tag{2}$$

Figure 1 shows the outlines of the contained plasma, vacuum vessel and TF coil.

A basic vacuum vessel is formed by top and bottom torispherical heads closed by inner and outer cylindrical walls. The torispherical heads are characterized by the average diameter D_v, the average radius of dish R_v, and the average outer and inner knuckle radii, $r_{v,o}$ and $r_{v,i}$, respectively. The Klöpper torispherical head or decimal head is defined by $R_v = D_v$ and $r_{v,o} = 0.1D_v$, while the standard Korbbogen torispherical head used in this report is defined by $R_v = 0.8D_v$ and $r_{v,o} = 0.154D_v$. The average diameter of the torispherical head is taken equal to $D_v = 2.000\,\mathrm{m}$ and the thickness of the outer cylindrical wall is $\Delta_v = 0.010\,\mathrm{m}$. The values of the inner cylindrical wall parameters are assumed to be: average diameter $d_v = 0.360\,\mathrm{m}$; total height $h_v = 1.700\,\mathrm{m}$; average knuckle radius $r_{v,i} = r_{v,o}/2 = 0.154\,\mathrm{m}$; and thickness $\delta_v = \Delta_v$. These dimensions are chosen in order to accommodate the plasma and possible divertors. The angle between the horizontal plane and the inner edge of dish (supplement of the angle included by the inner knuckle) is

$$\beta_v = \arccos\left(\frac{d_v/2 + r_{v,i}}{R_v - r_{v,i}}\right) = 1.3377\,\mathrm{rad}. \tag{3}$$

The dish center is located on the vertical axis at $(0, -Z_v)$ where

$$Z_v = (R_v - r_{v,i})\sin\beta_v - \frac{h_v}{2} = 0.5569\,\mathrm{m}. \tag{4}$$

The angle between the horizontal plane and the outer edge of dish (angle included by the outer knuckle) is

$$\alpha_v = \arccos\left(\frac{D_v/2 - r_{v,o}}{R_v - r_{v,o}}\right) = 1.0056\,\text{rad}, \tag{5}$$

and the total height of the outer cylindrical wall is

$$H_v = 2\left[(R_v - r_{v,o})\sin\alpha_v - Z_v\right] = 1.0683\,\text{m}. \tag{6}$$

The vacuum vessel is symmetric with respect to the equatorial plane. The upper half of the vacuum vessel centerline is represented in graphical form by: (**1**) a line joining the points $(D_v/2, 0)$ and $(D_v/2, H_v/2)$ (outer cylindrical wall); (**2**) a circular arc of radius $r_{v,o}$ centered at the point $(D_v/2 - r_{v,o}, H_v/2)$, with starting angle 0 and ending angle α_v (outer knuckle); (**3**) a circular arc of radius R_v centered at the point $(0, -Z_v)$ with starting angle α_v and ending angle β_v (upper dish); (**4**) a circular arc of radius $r_{v,i}$ centered at the point $(d_v/2 + r_{v,i}, h_v/2)$ with starting angle β_v, and ending angle π (inner knuckle); and (**5**) a line joining the points $(d_v/2, h_v/2)$ and $(d_v/2, 0)$ (inner cylindrical wall). The lines and arcs from (**1**) to (**4**) have a relative thickness $\Delta_v/\Delta R$ and the line (**5**) has a relative thickness $\delta_v/\Delta R$, where $\Delta R = 1.5\,\text{m}$ sets the scale of the graphics. The vacuum vessel centerline is displayed in Fig. 1.

The design of the center post of the TF coil involves various geometrical parameters defined as follows. First, the number of turns in the TF coil is taken equal to $N_t = 12$, dividing the center post in N_t sectors, and the inner radius of the central post is assumed equal to $r_{\min} = 0.050$ m. The outer radius of the center post, with small external clearance for a thin inboard shield is $r_{\text{rmax}} = 0.150\,\text{m}$. For a bare center post the outer radius can take the maximum value $r_{\max} = 0.170$ m. The minimum radius of the median (elastic) line of the TF coil for a shielded center post is

$$R_{\min} = \frac{r_{\min} + r_{\max}}{2} = 0.10\,\text{m}, \tag{7}$$

and the total cross-sectional area of each sector of the central column is

$$A_s = \frac{\pi}{N_t}\left(r_{\max}^2 - r_{\min}^2\right) = 0.005236\,\text{m}^2. \tag{8}$$

The cross-sectional area of each of the N_t trapezoidal copper bars that form the central column (including the area of the cooling holes) is

$$\begin{aligned} A_b \;=\; & \left[r_{\max}\cos\left(\frac{\pi}{N_t}\right) - (r_{\min} + t)\right]\left[r_{\max}\cos\left(\frac{\pi}{N_t}\right) + r_{\min}\right]\tan\left(\frac{\pi}{N_t}\right) \\ & -t\left[r_{\max} - (r_{\min} + t)\sec\left(\frac{\pi}{N_t}\right)\right] = 0.004513\,\text{m}^2, \end{aligned} \tag{9}$$

where $t = 0.003\,\text{m}$ is the thickness of the insulation layer between bars. The outer width of each trapezoidal copper bar is

$$b = 2\left[\left(r_{\max} - \frac{t/2}{\cos(\pi/N_t)}\right)\sin\left(\frac{\pi}{N_t}\right) - \frac{t/2}{\cos(\pi/N_t)}\right] = 0.07374\,\text{m}. \tag{10}$$

Considering the thickness $t_1 = 0.002\,\text{m}$ of the external insulation layer of the central column, the spacing between the TF coil and the vacuum vessel (TF coil – vacuum vessel clearence) is

$$s_1 = \left(\frac{d_v}{2} - \frac{\delta_v}{2}\right) - (r_{\max} + t_1) = 0.023\,\text{m}. \tag{11}$$

Finally, the spacing between the vacuum vessel and the plasma (vacuum vessel to plasma clearence) is

$$s_2 = (R_0 - a) - \left(\frac{d_v}{2} + \frac{\delta_v}{2}\right) = 0.015\,\text{m}. \tag{12}$$

Alternatively, the center post can be configured without a thin inboard shield, that is, a bare center column enclosed by insulation layers only. The number of turns in the TF coil, $N_t = 12$, and the inner radius, $r_{\min} = 0.050\,\text{m}$, maintain the previous values, but the outer radius increases to $r_{\max} = 0.170\,\text{m}$ giving a minimum median radius of the TF coil equal to

$$R_{\min} = \frac{r_{\min} + r_{\max}}{2} = 0.11\,\text{m}. \tag{13}$$

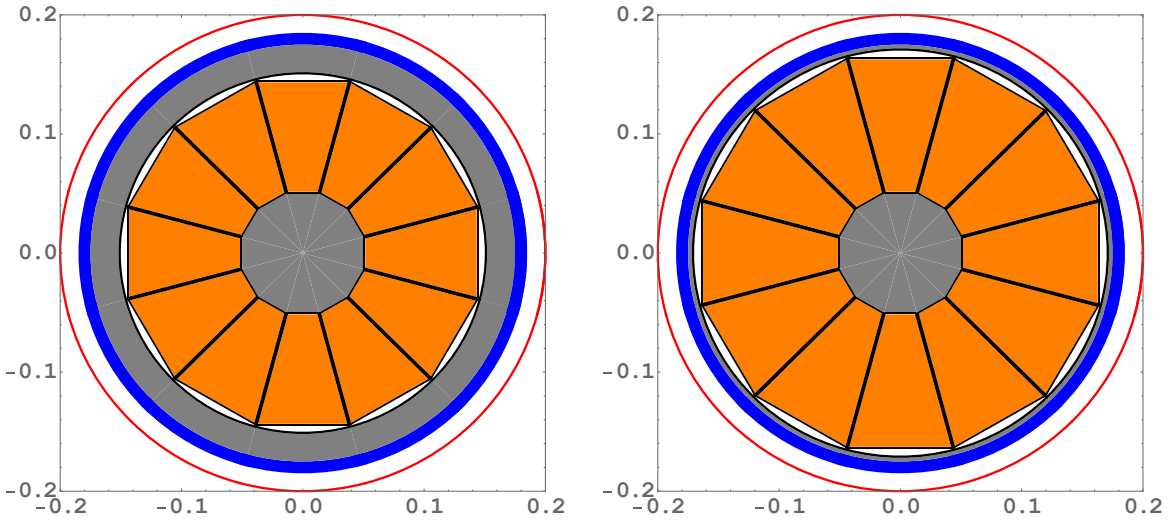

FIG. 2. Left picture: Center post of the toroidal field coil with small TF coil – vacuum vessel clearance for either a thin inboard shield or transformer solenoid. Right picture: Center post without an inboard shield. These pictures show the central post without cooling channels.

Accordingly, the minimal spacing between the TF coil and the vacuum vessel (TF coil – vacuum vessel clearance) is

$$s_1 = \left(\frac{d_v}{2} - \frac{\delta_v}{2}\right) - (r_{\max} + t_1) = 0.003\,\mathrm{m}, \tag{14}$$

where the thickness $t_1 = 0.002\,\mathrm{m}$ of the external insulation layer has the same previous value. The cross-sectional area of each of the trapezoidal copper bars becomes

$$\begin{aligned} A_b \;=\; & \left[r_{\max}\cos\left(\frac{\pi}{N_t}\right) - (r_{\min}+t)\right]\left[r_{\max}\cos\left(\frac{\pi}{N_t}\right) + r_{\min}\right]\tan\left(\frac{\pi}{N_t}\right) \\ & -t\left[r_{\max} - (r_{\min}+t)\sec\left(\frac{\pi}{N_t}\right)\right] = 0.006038\,\mathrm{m}^2, \end{aligned} \tag{15}$$

and the external width of each trapezoidal bar increases to

$$b = 2\left[\left(r_{\max} - \frac{t/2}{\cos\left(\pi/N_t\right)}\right)\sin\left(\frac{\pi}{N_t}\right) - \frac{t/2}{\cos\left(\pi/N_t\right)}\right] = 0.08409\,\mathrm{m}. \tag{16}$$

The cross-section of the center post of the TF coil is shown in Fig. 2 both for the thin inboard shield (left picture) and bare central column (right picture) configurations. The central column geometry shown in the right picture of Fig. 2, which corresponds to a center post without shield, will be considered throughout the remainder of this report. The bare center post configuration presents a larger cross-sectional copper area, adequate for the production of high toroidal magnetic fields in a small, low-power compact device.

The cross-section of the outer segments of the TF coil, for the bare central column with equivalent cross-sectional area, is formed by a rectangle of base b and height c given by

$$c = \frac{A_b}{b} = 0.07180\,\mathrm{m}. \tag{17}$$

Assuming that both the outer (rectangular) and inner (trapezoidal) segments of the TF coil have the same cooling holes area, they also have an equivalent copper area. This conditions the vanishing bending moment at the joints, between the inner and outer segments of the TF coil, for identical material properties and elastic line constants. Figure 3 illustrates one configuration where the cross-sections of the internal and external segments of the TF coil have the same effective copper area. Defining a fraction of the area that is copper by λ, the effective cross-sectional copper area of each segment is

$$A_c = \lambda A_b. \tag{18}$$

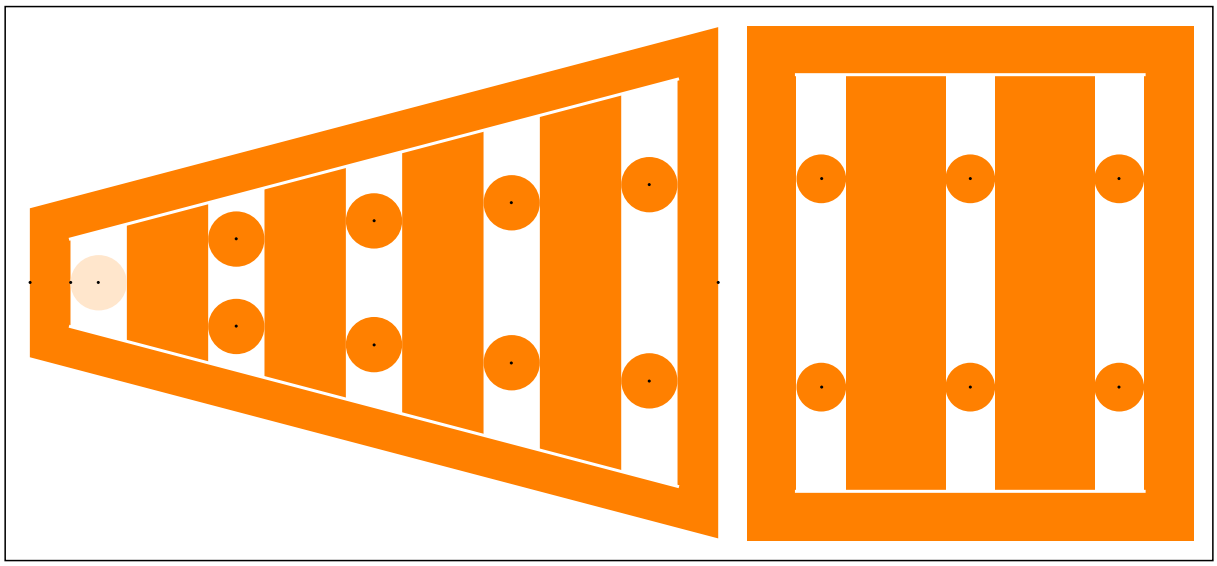

FIG. 3. Simplified cross-section representation of the inner (trapezoidal) and outer (rectangular) segments of the TF coil. The inner and outer segments are formed by long trapezoidal and rectangular curved copper bars, respectively, inserted in fitting copper enclosures and separated by long cylindrical copper rods. The conducting walls and bars should be grooved to fit the rods, and both segments have equivalent areas and the same copper fraction λ by design. The dimensions of the trapezoidal section must change continuously in the transition region between the inner and outer segments, up to the junction at the highest point of the TF coil.

A detailed presentation of the internal geometry of the TF coil segments will be deferred to Section III. The remaining of the present section is dedicated to a discussion of the overall geometry of the TF coil and simple adiabatic heating calculations.

The size and the shape of the TF coil are determined by the minimum median radius $R_{\min} = (r_{\min} + r_{\max})/2 = 0.11\,\mathrm{m}$ and the maximum median radius which is set as $R_{\max} = 1.30\,\mathrm{m}$. The elastic line constant is

$$k_t = \frac{1}{2}\ln\left(\frac{R_{\max}}{R_{\min}}\right) = 1.2348, \tag{19}$$

and the height of the central column is

$$H_t = 2\pi k_t \sqrt{R_{\min}R_{\max}}\, I_1(k_t) = 2.1793\,\mathrm{m}, \tag{20}$$

where I_1 is the modified Bessel function of the first kind and order one. The D-shaped centerline (elastic line) of the TF coil is described by the parametric equations

$$\begin{aligned} R_t &= \sqrt{R_{\min}R_{\max}}\exp(k_t\cos\theta), \\ Z_t &= k_t\sqrt{R_{\min}R_{\max}}\int_0^\theta \exp(k_t\cos\theta')\cos\theta'\,d\theta'. \end{aligned} \tag{21}$$

The left picture of Fig. 1 shows the TF coil represented by its centerline of variable width: the radial width is $r_{\max} - r_{\min} = 12.0\,\mathrm{cm}$ along the straight inner segment of total height $H_t = 2.1793\,\mathrm{m}$; and the lateral width is $c = 7.180$ cm along the outer segment whose centerline is given by eq. (21). This shape constitutes a moment-free TF coil, but the final design must incorporate supporting structures and transitions between the inner and outer segments. The radius of curvature of the outer segment is

$$\rho_t = k_t R_t = k_t\sqrt{R_{\min}R_{\max}}\exp(k_t\cos\theta), \tag{22}$$

and the highest point of the TF coil centerline is located at the geometric mean radius

$$\begin{aligned} R_m &= \sqrt{R_{\min}R_{\max}} = 0.3782\,\mathrm{m}, \\ Z_m &= \frac{\pi}{2}k_t R_m\left(I_1(k_t) + L_1(k_t) + \frac{2}{\pi}\right) = 1.2743\,\mathrm{m}, \end{aligned} \tag{23}$$

where L_1 is the modified Struve function of order one. The total length of the TF coil centerline is

$$\ell_t = 2\pi k_t R_m \left[I_0\left(k_t\right) + I_1\left(k_t\right)\right] = 6.3429\,\mathrm{m}, \tag{24}$$

where I_0 is the modified Bessel function of the first kind and order zero. The half-length position is defined by the root θ of the equation

$$\ell\left(\theta\right) = k_t R_m \int_0^{\theta} \exp\left(k_t \cos\theta'\right) d\theta' = \ell_t/4, \tag{25}$$

so that $R_t\left(\theta\right) = 0.5123\,\mathrm{m}$ and $Z_t\left(\theta\right) = 1.2567\,\mathrm{m}$. The half-length position along the centerline is indicated by points on every turn of the TF coil in Fig. 1. The poloidal area enclosed by the TF coil (area delimited by the centerline perimeter) is

$$A_t = 2\pi k_t R_m^2 \left[I_1\left(2k_t\right) - \exp\left(-k_t\right) I_1\left(k_t\right)\right] = 2.4766\,\mathrm{m}^2, \tag{26}$$

and the inductance of the N_t turns toroid is ($\mu_0 = 4\pi \times 10^{-7}\,\mathrm{H\ m^{-1}}$)

$$L_{TF} = \mu_0 k_t R_m N_t^2 \left[k_t I_0\left(k_t\right) + \left(k_t - 1\right) I_1\left(k_t\right)\right] = 0.1628\,\mathrm{mH}. \tag{27}$$

The mass of copper (not taking into account joints and leads) is estimated by (assuming $\lambda = 0.78$)

$$m_c = \rho_c N_t \ell_t A_c = 3202.0\,\mathrm{kg}, \tag{28}$$

where $\rho_c = 8933\,\mathrm{kg\ m^{-3}}$ is the density of copper.

The toroidal magnetic field ripple at the plasma edge (equatorial plane) can be estimated by

$$\Delta = \frac{\left[\left(R_0 + a\right)/R_{\min}\right]^{N_t}}{\left[\left(R_0 + a\right)/R_{\min}\right]^{N_t} - 1} + \frac{\left[\left(R_0 + a\right)/R_{\max}\right]^{N_t}}{1 - \left[\left(R_0 + a\right)/R_{\max}\right]^{N_t}} - 1 = 0.002958. \tag{29}$$

For $R_{\max} > R_0 + a > R_{\min}$ and $N_t \gg 1$

$$\Delta \cong \left(\frac{R_0 + a}{R_{\max}}\right)^{N_t} = 0.002950. \tag{30}$$

For producing a toroidal magnetic field $B_0 = 3\,\mathrm{T}$ (maximum design value) at the geometrical plasma center (R_0, 0) the total current in each turn of the TF coil is

$$I_t = \frac{2\pi R_0 B_0}{\mu_0 N_t} = 625\,\mathrm{kA} \quad \left(N_t I_t = 7.5\,\mathrm{MA\ turn}\right), \tag{31}$$

and the current density for $B_0 = 3\,\mathrm{T}$ and $\lambda = 0.78$ is

$$j_t = \frac{I_t}{A_c} = 132.7\,\mathrm{MA\ m^{-2}}. \tag{32}$$

Accordingly, the electromagnetic force of tension along the TF coil is

$$F_t = \frac{\mu_0 N_t I_t^2}{4\pi} k_t = 578.8\,\mathrm{kN}, \tag{33}$$

giving an average stress

$$\sigma_t = \frac{F_t}{A_c} = 122.9\,\mathrm{MPa}. \tag{34}$$

The admissible stress for oxygen-free hard temper copper with yield strength $\sigma_y = 274\,\mathrm{MPa}$ is $\sigma_{\mathrm{adm}} = 183\,\mathrm{MPa}$. The design criterion is $\sigma_{\mathrm{adm}} \leq (2/3)\,\sigma_y$. The yield strength of oxygen free half-hard copper is $\sigma_y = 186\,\mathrm{MPa}$ and for Glidcop is $\sigma_y = 310\,\mathrm{MPa}$.

Assuming adiabatic heating of the TF coil, the temperature rise of the conductor during the current pulse is governed by the equation

$$\rho_c C_{p,c} \frac{dT_c}{dt} = \eta_c j_t^2, \tag{35}$$

where $C_{p,c} = 385\,\mathrm{J\ kg^{-1}\ K^{-1}}$ is the specific heat of copper at $T_0 = 25\,^\circ\mathrm{C}$. The resistivity of copper corrected for temperature T_c is

$$\eta_c = \eta_0 \left(1 + \alpha_T T_c\right), \tag{36}$$

where $\eta_0 = 0.0159\,\mu\Omega$ m is the resistivity at $T_c = 0\,^\circ\mathrm{C}$ and $\alpha_T = 0.00423\,\mathrm{K^{-1}}$ is the temperature coefficient. Integration of the temperature evolution equation gives

$$\int_0^\infty j_t^2\,(t)\,dt = \frac{\rho_c C_{p,c}}{\eta_0}\frac{1}{\alpha_T}\ln\left(\frac{1+\alpha_T T_\infty}{1+\alpha_T T_0}\right). \tag{37}$$

Defining the effective pulse length for adiabatic heating by

$$t_{\mathrm{eff}} = \frac{1}{j_t^2}\int_0^\infty j_t^2\,(t)\,dt, \tag{38}$$

the conductor temperature $T_c = T_\infty$ at the end of the current pulse is calculated using the formula

$$T_\infty = \frac{1}{\alpha_T}\left[(1+\alpha_T T_0)\exp\left(\alpha_T\frac{\eta_0}{\rho_c C_{p,c}} j_t^2 t_{\mathrm{eff}}\right) - 1\right]. \tag{39}$$

This expression indicates that for $B_0 = 3\,\mathrm{T}$ the effective pulse length must be limited to $t_{\mathrm{eff}} \sim 2.1\,\mathrm{s}$ in order to keep the conductor temperature below $\sim 300\,^\circ\mathrm{C}$ (the melting temperature of copper, $T_c = 1085\,^\circ\mathrm{C}$, is reached in 4.7 s). Reducing the magnetic field to $B_0 = 1\,\mathrm{T}$, the effective pulse length can be extended to $t_{\mathrm{eff}} \sim 19\,\mathrm{s}$ for $T_c \lesssim 300$. If the TF coil is pre-cooled to cryogenic temperature $-196\,^\circ\mathrm{C}$ the effective pulse length can be extended, for $B_0 = 3\,\mathrm{T}$, to $\sim 7.5\,\mathrm{s}$. In all cases the temperature variation is limited by the insulation heat resistance: RP-46 polyimide has high heat resistance from -101 to $393\,^\circ\mathrm{C}$ (RP-46 polyimide/glass composite high-resistance insulation withstand a 3-hour gas-flame test at $871\,^\circ\mathrm{C}$).

The electric resistance of the TF coil, not taking into account joints and leads, can be estimated by

$$R_{TF} = \eta_c N_t \frac{\ell_t}{A_c}, \tag{40}$$

and the voltage drop at the beginning and end of a current pulse for $B_0 = 3\,\mathrm{T}$ and $\lambda = 0.78$ becomes

$$V_{TF} = R_{TF} I_t = \begin{cases} 174.2\,\mathrm{V} & (T_c = T_0 = 20\,^\circ\mathrm{C}) \\ 364.4\,\mathrm{V} & (T_c = T_\infty = 300\,^\circ\mathrm{C}) \end{cases} \tag{41}$$

The thermal calculations for adiabatic heating indicate that for significant pulse lengths the cooling system of the TF coil (the center post in particular) must be designed for steady-state operation. The requirements for cooling the TF coil are examined in the next section.

III. TOROIDAL FIELD COIL COOLING

This section addresses the limits imposed by cooling the TF coil, in the bare center post configuration shown in the right picture of Fig. 2, for a toroidal magnetic field in the range $1.0 \sim 3.0\,\mathrm{T}$. The cooling system consists of $2N_t = 24$ independent parallel circuits formed by dividing each turn of the TF coil in two equal-length circuits interrupted at the upper (and lower) positions indicated by the points in Fig. 1. The coolant enters at the upper part and is collected at the lower end of each turn of the TF coil. Note that the turns of the TF coil can be electrically connected in series at these same positions. Since the inner and outer segments have the same length $\ell_t/2 = 3.1714\,\mathrm{m}$, cross-sectional area $A_b = 60.38\,\mathrm{cm^2}$, and copper fraction λ, the analysis of the cooling system can be reduced to a single cooling channel.

The cooling channels geometry, for the outer segments of the TF coil, is shown in the right picture of Fig. 3. As described in the caption of this figure, the outer segment is formed by long curved copper bars of rectangular cross-section, separated by thin cylindrical copper rods. The interstitial rods are represented in a simplified form, but should be wedged in the rectangular bars. The entire set of bars and rods is inserted in a rectangular casing wall. Each rectangular inner bar has a width $b - 2e$ and height $2e$. Here, $b = 8.409\,\mathrm{cm}$ is the previously calculated overall width of each rectangular outer segment of the TF coil (cf. Section II). The overall height of the rectangular segments is $c = A_b/b = 7.180\,\mathrm{cm}$. The wall thickness of the copper casing is also taken equal to e, not yet defined, and the diameter of each

cylindrical rod is d. Assuming that there are N_c cooling channels ($N_c = \text{Integer}$), and taking into account the copper fraction λ, these dimensions are related by:

$$\begin{aligned} d &= \frac{b}{\pi-2}\left[1-\frac{A_b}{N_c b^2}-\sqrt{\left(1+\frac{A_b}{N_c b^2}\right)^2-2\frac{A_b}{N_c b^2}\left[\pi-(\pi-2)\,\lambda\right]}\right], \\ e &= \frac{b}{2\,(\pi-2)}\left[\frac{A_b}{N_c b^2}\,(\pi-1)-1+\sqrt{\left(1+\frac{A_b}{N_c b^2}\right)^2-2\frac{A_b}{N_c b^2}\left[\pi-(\pi-2)\,\lambda\right]}\right]. \end{aligned} \tag{42}$$

As will be shown later, a nearly optimal design is obtained with $d = e$, which corresponds to a copper fraction

$$\lambda = \frac{2}{3}+\frac{(4+\pi)\,A_b}{18 N_c b^2}. \tag{43}$$

In particular, $N_c = 3$ gives

$$d = e = 7.978\,\text{mm} \quad \text{and} \quad \lambda \simeq 0.780. \tag{44}$$

The hydraulic diameter of the N_c cooling channels is given in terms of the cross-sectional area of the flow, A, and the wetted perimeter of the cross-section, P, of each channel by

$$D = \frac{4A}{P} = \frac{4\,(1-\lambda)\,A_b}{2N_c\,(b-2e+d+\pi d)} = \frac{2\,(b-2e)\,d-\pi d^2}{b-2e+d+\pi d}. \tag{45}$$

For $N_c = 3$ and $\lambda = 0.780$ the hydraulic diameter is $D = 8.769\,\text{mm}$. The average distance to the nearest cooling surface is approximately given by $e = 7.978\,\text{mm}$, and the geometrical representation corresponding to these values is shown in the right side of Fig. 3.

The geometry of the trapezoidal inner segments, shown in the left side of Fig. 3, can be calculated in terms of the extreme points:

$$\begin{aligned} x_1 &= r_{\min}+\frac{t}{2}, \\ y_1 &= \left(r_{\min}+\frac{t}{2}\right)\tan\left(\frac{\pi}{N_t}\right)-\frac{t/2}{\cos\left(\pi/N_t\right)}, \\ x_2 &= r_{\max}\cos\left(\frac{\pi}{N_t}\right)-\frac{t}{2}, \\ y_2 &= \left(r_{\max}-\frac{t/2}{\cos\left(\pi/N_t\right)}\right)\sin\left(\frac{\pi}{N_t}\right)-\frac{t/2}{\cos\left(\pi/N_t\right)}, \end{aligned} \tag{46}$$

so that the external area of each trapezoidal copper bar is given by

$$A_{\text{ext}} = (x_2-x_1)\,(y_1+y_2)\,, \tag{47}$$

and the area of the internal trapezoid is (this is the area A_{ext} reduced by the thickness e_1 of the trapezoidal containing wall)

$$A_{\text{int}} = (x_2-x_1-2e_1)\left[y_1+y_2-2e_1\sec\left(\frac{\pi}{N_t}\right)\right]. \tag{48}$$

Furthermore, defining the extreme internal points

$$\begin{aligned} x_3 &= r_{\min}+\frac{t}{2}+e_1, \\ y_3 &= \left(r_{\min}+\frac{t}{2}+e_1\right)\tan\left(\frac{\pi}{N_t}\right)-\frac{t/2+e_1}{\cos\left(\pi/N_t\right)}, \\ x_4 &= r_{\max}\cos\left(\frac{\pi}{N_t}\right)-\frac{t}{2}-e_1, \\ y_4 &= \left(r_{\max}-\frac{t/2+e_1}{\cos\left(\pi/N_t\right)}\right)\sin\left(\frac{\pi}{N_t}\right)-\frac{t/2+e_1}{\cos\left(\pi/N_t\right)}, \end{aligned} \tag{49}$$

the total area of the N_1-1 internal trapezoidal slabs of thickness $2e_1$ is given by (N_1 is the integer number of cooling channels in the trapezoidal segments of the TF coil)

$$A_{\text{slabs}} = 2\,(N_1-1)\,e_1\left[2y_4-\left(N_1 d_1+2e_1\,(N_1-1)\,\frac{y_4-y_3}{x_4-x_3}\right)\right]. \tag{50}$$

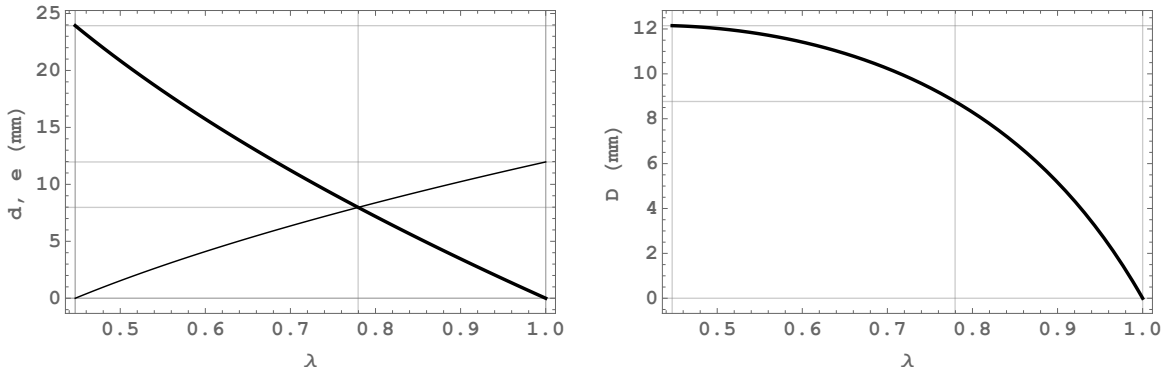

FIG. 4. Variation of the cooling channels width, d (thick line), and of the copper bands half-width, e (thin line), as a function of the copper fraction $\pi A_b/\left(2N_c b^2\right) \leq \lambda \leq 1$ for $N_c = 3$ (left picture). Variation of the hydraulic diameter, D, as a function of λ (right picture). The thin vertical lines indicate the value $\lambda = 2/3 + (4+\pi)\, A_b/\left(18 N_c b^2\right)$ for which $d = e = A_b/\left(3N_c b\right)$.

Finally, the total area of the $2N_1$ internal cylindrical separating rods of diameter d_1 is

$$A_{\rm rods} = 2\,(N_1 - 1)\,\frac{\pi d_1^2}{4}, \tag{51}$$

so that the copper fraction of the inner trapezoidal segments is simply given by

$$\lambda_1 = \frac{(A_{\rm ext} - A_{\rm int}) + A_{\rm slabs} + A_{\rm rods}}{A_{\rm ext}}. \tag{52}$$

The above formulas allow to calculate d_1 and e_1 so that, for given $N_1 > N_c$, the total number of inserts cover the available space $x_4 - x_3$ and the inner and outer segments have the same copper fraction $\lambda_1 = \lambda$:

$$\begin{array}{rcl} x_4 - x_3 & = & N_1\,(d_1 + 2e_1) - 2e_1, \\ \lambda_1 & = & \lambda. \end{array} \tag{53}$$

The dimensions b and e, and the hydraulic diameter, D, are functions of the integer number of cooling holes, N_c, and of the copper fraction, λ. Figure 4 shows, for $N_c = 3$, the variation of b, e and D as a function of λ.

For $N_c = 3$, $N_1 = 5$ and $\lambda_1 = \lambda = 0.780$, the components of the outer and inner segments of the TF coil have the following final dimensions, as shown in Fig. 3:

$$\begin{array}{rclcrcl} b & = & 84.09\,{\rm mm} & , & c & = & 71.80\,{\rm mm}, \\ d & = & 7.978\,{\rm mm} & , & e & = & 7.978\,{\rm mm}, \\ d_1 & = & 9.099\,{\rm mm} & , & e_1 & = & 6.571\,{\rm mm}. \end{array} \tag{54}$$

Some additional adjustments can be made so that the inner and outer segments have cooling holes with nearly the same hydraulic diameter, avoiding pressure drop unbalance, but this refinement is not presently needed. The cooling requirement analysis in this report will be made based on the above reference design of the outer segment of the TF coil. A few alternative configurations for the cooling holes geometry are presented in the Appendix C.

Considering the local heat input density $\eta_c j_t^2$ and the total copper volume of the TF coil, $V = 2N_t L A_c$, where $L = \ell_t/2$ is the length of the cooling channels, the total power (in W) deposited in the cooling circuits is

$$W = \eta_c j_t^2 V = \frac{\eta_c \ell_t}{N_t A_b \lambda}\left(\frac{2\pi R_0 B_0}{\mu_0}\right)^2, \tag{55}$$

which depends on the average temperature T_c of the conductor. Note that the TF coil is formed by $2N_t$ hydraulic circuits in parallel. For cooling circuits with a cross-sectional area of the flow $A_b - A_c = A_b\,(1-\lambda)$, the total discharge (volume flow of water in $\rm m^3\ s^{-1}$) in the cooling circuits is given by

$$Q = 2N_t A_b\,(1-\lambda)\,u = 2N_t A_b\,(1-\lambda)\,\frac{G}{\rho}, \tag{56}$$

where u is the mean velocity of the fluid, $G = \rho u$ is the mean mass flux in the channel, and ρ is the fluid density (c.f. Appendix A). According to the definition of the mean temperature T_l of the fluid, given in Appendix A, the steady-state fluid temperature rise along each cooling circuit is

$$\Delta T_l = \frac{W}{C_p \dot{m}}, \tag{57}$$

where C_p is the specific heat capacity at constant pressure of the coolant, and $\dot{m} = \rho Q = 2N_t A_b (1-\lambda) G$ is the total mass flow rate (in kg s^{-1}) in the circuit. The fluid temperature along the cooling channel of total length L increases linearly with distance z from the input

$$T_l = T_0 + \Delta T_l \frac{z}{L}. \tag{58}$$

Now, considering the effective transverse distance for heat conduction ℓ, the one-dimensional estimate of the hot-spot temperature rise inside the conductor is

$$\Delta T_c = \frac{\eta_c j_t^2 \ell^2}{2k_c} = \frac{W \ell^2}{2k_c V}, \tag{59}$$

where $k_c = 401\,\mathrm{W\ m^{-1}\ K^{-1}}$ is the thermal conductivity of copper at 20 °C. Assuming a parabolic temperature profile, the average surface temperature of the conductor is

$$T_s = T_c - \frac{2\Delta T_c}{3}. \tag{60}$$

Accordingly, the maximum temperature inside the conductor is estimated by

$$T_{\max} = T_c + \frac{\Delta T_c}{3}. \tag{61}$$

The boundary layer temperature difference is $\Delta T_b = T_s - T_l$, where T_l is the cooling fluid mean temperature ($T_l < T_s < T_c$).

Taking into account the perimeter $P = 2N_c [b - 2e + (1+\pi) d]$ and the total surface $2N_t PL$ of the cooling channels, the heat flux input (in W m^{-2}) in each channel is

$$q_i = \frac{W}{2N_t PL} = \frac{\eta_c j_t^2 A_c}{P}, \tag{62}$$

which depends on the geometry, magnetic field B_0 and average temperature T_c of the conductor. The heat flux output is

$$q_o = h \Delta T_b, \tag{63}$$

where $\Delta T_b = T_s - T_l$ is the previously defined boundary layer temperature difference, h is the convection heat transfer coefficient given by the Gnielinski correlation (A12) including the Petukhov property correction factor (A17)

$$h = \frac{k}{D} \frac{(f_D/8)\,(\mathrm{Re} - 1000)\,\mathrm{Pr}}{1 + 12.7\,(f_D/8)^{1/2} \left(\mathrm{Pr}^{2/3} - 1\right)} \left(\frac{\mu}{\mu_s}\right)^{0.11}, \tag{64}$$

and the friction factor f_D is calculated by the Churchill eq. (A16). The heat flux output depends on geometry (including surface roughness ε), magnetic field B_0, mean mass flux G, average temperature T_c of the conductor, and mean fluid temperature T_l. The temperatures T_l and T_c can be determined consistently, at each position $0 \le z \le L$ along the cooling channel, solving the equations

$$\begin{cases} T_l &= T_0 + \Delta T_l \dfrac{z}{L} \\ q_i &= q_o \end{cases} \tag{65}$$

Accordingly, the average power deposited in the TF coil circuit is given by

$$\overline{W} = \frac{V}{L} \int_0^L \eta_c j_t^2 dz = 2N_t A_c \int_0^L \eta_c j_t^2 dz = 2N_t P \int_0^L q_i\, dz = 2N_t P \int_0^L q_o\, dz. \tag{66}$$

B_0 (T)	u_0 (m/s)	T_s (°C)	T_c (°C)	W (MW)	$\overline{W}$ (MW)	Q (m^3/s)	p_0 (bar)	Δp (bar)	P_h (kW)
1.0	1.608	127.3	129.9	17.29	15.42	0.05349	2.61	0.1210	0.6472
2.0	6.709	134.9	145.6	72.12	64.40	0.2231	4.56	1.651	36.83
3.0	15.87	140.1	165.3	170.6	152.6	0.5279	12.67	8.159	430.7

TABLE I. Cooling system parameters corresponding to the operating points indicated in Fig. 5, for both fixed copper fraction $\lambda = 0.780$ and output average fluid temperature $T_l = 100\,^{\circ}\mathrm{C}$.

The pressure drop along the central column of the TF coil is expressed by the Darcy-Weisbach equation (c.f. Appendix A)

$$\Delta p = \left(\frac{1}{2\rho_0} + \frac{f_D}{\rho}\frac{z}{d}\right)\frac{G^2}{2}\left[H\left(z\right) - H\left(z-L\right)\right] + \left(\frac{1}{2\rho_0} + \frac{1}{\rho_L} + \frac{f_{D,L}}{\rho_L}\frac{L}{d}\right)\frac{G^2}{2}H\left(z-L\right), \tag{67}$$

where $H\left(z\right)$ denotes the Heaviside step function and the L subscript refers to the conditions at the end of the channel $z = L = \ell_t/2$. The initial factor $1/2\rho_0$ corresponds to the full entrance head loss and the additional factor $1/\rho_L$ to the exit loss. Accordingly, the pressure along the cooling channel varies as

$$p = p_0 - \Delta p, \tag{68}$$

where p_0 is the input pressure. The ideal pumping power (not taking into account the pump efficiency) is given by Bernoulli's equation

$$P_h = Q\Delta p. \tag{69}$$

Figure 5 shows the variation of the fluid temperature T_l and of the power W dissipated in the TF coil, at the output of the cooling channels, as functions of the input flow velocity u_0 and the copper fraction varying from $\lambda = 0.65$ to $\lambda = 0.85$. The rows in Fig. 5 correspond, from top to bottom, to the magnetic field values $B_0 = 1.0, 2.0$ and $3.0\,\mathrm{T}$, respectively, for flows in smooth pipes with absolute roughness $\varepsilon = 0$. In each case, the central points displayed in the graphics correspond to the value of the input flow velocity u_0 compatible with an output temperature $T_l = 100\ ^{\circ}\mathrm{C}$ for fixed copper fraction $\lambda = 0.780$. These values are fixed to allow comparison of the cooling requirements and dissipated power for the different values of the magnetic field. Note the change in scale for the flow velocity u_0, in m/s, and the dissipated power W, in MW. Note also that the value of the copper fraction $\lambda = 0.780$ corresponds approximately to the minimum value of the dissipated power for $T_l = 100\,^{\circ}\mathrm{C}$ (a slight improvement main be obtained for $\lambda \simeq 0.80$). Table I lists the operating conditions corresponding to the central points displayed in Fig. 5, including the output values of the surface conductor temperature T_s and of the average conductor temperature T_c, as well as the total average power $\overline{W}$ dissipated in the TF coil, output discharge Q, input pressure p_0, total pressure drop Δp in each channel, and total pumping power P_h. The pumping power includes the full entrance and exit head losses.

Figure 6 shows the variation of the fluid and conductor temperatures along the cooling channels of the TF coil. The magnetic flux density is equal to $B_0 = 1.0, 2.0$ and $3.0\,\mathrm{T}$ in the first, second and third rows, respectively. The copper fraction is assumed equal to the near optimum value $\lambda = 0.780$, defined by equation (43), and the constant mean mass flux $G = \rho u$ is defined by both the fluid temperature $T_0 = 20\,^{\circ}\mathrm{C}$ and the mean fluid velocity u_0 at the cooling channels entrance. The first column gives the results for smooth cooling ducts with $\varepsilon = 0$, while the second column gives the results for rough ducts with $\varepsilon = 10\,\mu\mathrm{m}$. The fluid temperature at the entrance is low and so is the heat transfer coefficient, but the boundary layer temperature difference is relatively large. For approximately constant heat flux along the channel wall (not exactly constant due to the change in the conductor resistivity) the fluid temperature rises almost linearly along the channel, resulting in an increase in the heat transfer coefficient and a corresponding decrease in the boundary layer temperature difference. The input flow velocity u_0 in Fig. 6 is adjusted so that the average fluid temperature reaches $T_l = 100\,^{\circ}\mathrm{C}$ at the end of the smooth cooling pipes, as listed in Table I. In general, depending on fluid flow velocity and pressure, the fluid temperature T_l can be maintained below the boiling point. However, in order to avoid boiling incipience the surface temperature of the conductor $T_s > T_l$ must be also below the saturation temperature. For fixed mass flux input, this condition can be attained by increasing the input pressure. Between $100\,^{\circ}\mathrm{C}$ and the critical temperature $374\,^{\circ}\mathrm{C}$, liquid water is in the superheated regime with overpressure up to the critical point 220 bar. As shown in Fig. 6, the saturation temperature decreases due to the pressure drop along the channels. Moreover, this figure clearly shows that the input pressure p_0 can be adjusted so that the temperature, at the conductor surface, is less than the saturation temperature of water everywhere inside the cooling channel, avoiding incipient boiling. Note that there is an initial head loss (not shown) at the entrance of the cooling channels. Note also that the pressure drop is larger for rough channels with

	1.0 T					2.0 T					3.0 T				
$\varepsilon = 0$	T_l	T_s	T_c	$T_{\max}$	$T_{\rm sat}$	T_l	T_s	T_c	$T_{\max}$	$T_{\rm sat}$	T_l	T_s	T_c	$T_{\max}$	$T_{\rm sat}$
$z = 0.00\,$m	20.0	58.1	60.1	61.2	128.6	20.0	65.0	73.6	78.0	147.1	20.0	70.3	90.8	101.1	187.2
$z = 3.17\,$m	100.0	**127.3**	129.9	131.2	**127.3**	100.0	**134.9**	145.6	150.9	**134.9**	100.0	140.1	165.3	177.9	157.2
$\varepsilon = 10\,\mu$m	T_l	T_s	T_c	$T_{\max}$	$T_{\rm sat}$	T_l	T_s	T_c	$T_{\max}$	$T_{\rm sat}$	T_l	T_s	T_c	$T_{\max}$	$T_{\rm sat}$
$z = 0.00\,$m	20.0	56.1	58.1	59.1	128.6	20.0	59.3	67.8	72.0	147.1	20.0	60.6	80.5	90.5	187.2
$z = 3.17\,$m	98.9	122.4	124.9	126.2	127.1	97.5	122.9	133.2	138.4	128.7	96.3	**122.2**	146.2	158.2	**122.2**

TABLE II. Distribution of temperatures in °C at the initial and end points of the cooling channels, for smooth ($\varepsilon = 0$) and rough ($\varepsilon = 10\,\mu$m) pipes.

$\varepsilon \sim 10\,\mu$m, resulting in a larger saturation temperature decrease. For relatively low flow velocities this decrease is compensated by the larger value of the heat transfer coefficient, so that both the average fluid and conductor surface temperatures remain below the saturation value along the channels. However, for high flow velocities in rough channels, as illustrated in the last picture of Fig. 6 ($B_0 = 3.0\,$T), the input pressure must be increased in order to have $T_s \le T_{\rm sat}$ at the end of the cooling channels. Figure 6 shows that the maximum temperature (hot-spot) in the conductor is also well below the temperature limit allowed for the insulation.

Table II lists the average fluid temperature, T_l, the surface, average and maximum conductor temperatures, T_s, T_c and $T_{\max}$, respectively, and the saturation temperature, $T_{\rm sat}$, at the initial and end points of the cooling channels, both for smooth and rough pipes, as shown in Fig. 6. The input flow velocity is adjusted in each case so that $T_l = 100$°C at the end point of smooth channels, while the input pressure is adjusted so that $T_s \le T_{\rm sat}$ for either smooth or rough channels, keeping the same value of the input flow velocity.

Figures 7, 8 and 9 show the performance of the cooling system of the TF field coil, for $\lambda = 0.780$ and $B_0 = 1.0, 2.0$ and $3.0\,$T, respectively, as a function of the input fluid velocity u_0. The fluid velocity is the single most important quantity in the cooling system performance. The velocity varies weakly along the length of the cooling channels, for constant mass flux, due to the weak dependence of the density on the fluid temperature. The discharge is simply proportional to the fluid velocity for fixed geometry. The total power varies with the conductor temperature, which depends mainly on the fluid velocity and somewhat on the pipe roughness. According to the Darcy-Weisbach equation, the pressure loss due to viscous effects depends on the product of the fluid density, the squared fluid velocity and the Darcy friction factor, resulting in a nearly linear pressure drop along the channel. The pumping power is given by the product of the discharge and the total pressure loss. These figures show that the performance can be adjusted by modifying the indicated operating points. In particular, in the reduced magnetic field operation ($B_0 \le 2.0\,$T) the dissipated power can be somewhat reduced by increasing the flow velocity. In the high field case ($B_0 \cong 3.0\,$T) the flow velocity is already at a very high value. In all cases the cooling requirements are within the pressure and discharge rates of single-stage centrifugal pumps.

In this report it was assumed that the inner and outer segments of the TF coil have equivalent areas, leading to similar cooling requirements. Nevertheless, the dissipated power can be reduced by increasing the copper area of the outer segments. Since, in the present configuration, the power is equally divided in two segments, the power in the new configuration would be given by

$$\overline{W}_{\rm new} = \frac{\overline{W}}{2}\left(1 + \frac{1}{A_{\rm ext}/A_{\rm int}}\right), \tag{70}$$

where $A_{\rm ext}/A_{\rm int}$ is the ratio of the cross-sections of external and internal segments. This indicates that the total power can be substantially reduced by enlarging the cross-sectional area of the external segments. In this case, the transition between the inner and outer segments requires a detailed stress analysis. Also, the coils assembly could be simplified by considering a straight central column connected to the outer legs by sliding joints. Nevertheless, the cooling requirements for the central post would be the same as analyzed for the half-length TF coil, assuming that the length $L = \ell_t/2$ is the same if cooling entrances are included. Alternative configurations for the cooling channels in the center post are briefly discussed in the Appendix C.

IV. CONCLUSIONS AND COMMENTS

The main conclusion is that the steady-state cooling requirements for the large diameter (bare) center post can be attained with somewhat high values of the temperature (conductor temperature < 165°C), and quite demanding levels of input fluid flow velocity $u_0 \cong 16\,$m/s, input pressure $p_0 \cong 13\,$bar and

pumping power $P_h \cong 431\,\mathrm{kW}$ for a 3.0 T magnetic induction at the plasma center. The total average power dissipated in the TF coil is $\overline{W} \cong 153\,\mathrm{MW}$. The cooling system requisites are considerably reduced for $B_0 = 2.0\,\mathrm{T}$, namely $T_c < 146°\mathrm{C}$, $u_0 \cong 6.7\,\mathrm{m/s}$, $p_0 \cong 4.6\,\mathrm{bar}$ and $P_h \cong 37\,\mathrm{kW}$ resulting in $\overline{W} \cong 65\,\mathrm{MW}$. Of course, the electric power requirements to sustain the magnetic field are very high, so that true steady state without superconducting coils is feasible only for low values of the field, possibly $B_0 \leq 2\,\mathrm{T}$ with optimized configuration of the TF coil. Nevertheless, a proper cooling system is necessary for long pulse operation (cf. Section II).

In the bare center post configuration no space remains between the central column and the vacuum vessel (a mere 3 mm gap remains). In this case there is practically no space available for joints and water inlets near the center post. One possibility, advanced in the present report, is to displace the joints outwards along the TF coil legs. The TF coils can be fabricated as single pieces, welding the vacuum chamber afterwards inside the coil. The assembly of the vacuum vessel could be started welding a flared cylinder tightly around the central column and then welding the outer pieces. Alternatively, for a straight central column the outer legs of the TF coil could be connected trough sliding joints, with increased cross-sectional area.

The analysis of the cooling system used correlations for the heat transfer coefficient in a simplified geometry of the center post, and a one-dimensional approximation for heat conduction. This analysis can be improved using a two-dimensional calculation of the transverse heat conduction in copper, and a time dependent simulation. The copper properties dependence with temperature can also be improved in the model.

A final comment concerns the analysis of the central column cooling problem developed in reference [1]. Although it is not expressly stated in the paper, the authors completely ignored the temperature difference across the boundary layer of the cooling fluid. In other words, they implicitly assumed that the temperature on the surface of the cooling channel is equal to the average temperature of the fluid, resulting in overall small temperature differences and low fluid velocity in the cooling system. Actually, the temperature difference in the boundary layer corresponds to a substantial transverse contribution in the problem at hand, as clearly shown in Fig. 6. The steady state operation of the central column is feasible with large flow velocities, but a 9 T steady state magnetic field is ruled out in a water cooled compact device: $\sim 3.5\,\mathrm{T}$ seems to be close to the limit, using high-strength materials and very-high pumping capability, with a very-high total power dissipation in the central column only. A magnetic field $B_0 = 4\,\mathrm{T}$ surpasses the admissible stress for hard temper copper, in the present geometry, requiring Glidcop or other high-strength materials for compact design. The high-pressure operation is needed to avoid boiling inside the channel, but this condition can be somewhat relaxed if the coolant is allowed to flow in the forced convection boiling flow regime. But, this regime will be examined in a separate report.

Appendix A: Correlations of the convective heat-transfer coefficient and the friction factor for water in turbulent flow

The analysis of heat transfer for turbulent flow conditions in a pipe involves three dimensionless quantities:

$$\begin{aligned} \mathrm{Re} &= GD/\mu, \\ \mathrm{Pr} &= C_p\mu/k, \\ \mathrm{Nu} &= hD/k, \end{aligned} \tag{A1}$$

the Reynolds, Prandtl and Nusselt numbers, respectively. Here, $G = \rho u$ is the mean mass flux in the cooling channel (mean mass flow rate per unit cross-sectional area in $\mathrm{kg\,m^{-2}\,s^{-1}}$), u is the mean velocity of the fluid (density-weighted average velocity over the cross section) and D is the hydraulic diameter of the pipe. In general, the fluid density ρ, the specific heat capacity C_p, the dynamic viscosity μ, and the thermal conductivity k are functions of the mean temperature T of the fluid. The convection heat transfer coefficient at a position along the flow is $h = (k/D)\,\mathrm{Nu}$.

The hydraulic diameter is given by

$$D = \frac{4A}{P}, \tag{A2}$$

where $A = \int_A dA$ is the pipe cross section area, and P is the wetted perimeter.

The mean velocity u is defined such that, when multiplied by the fluid density ρ and the cross-sectional area of the pipe A, it gives the total rate of mass flow $\dot{m}$ through the pipe

$$\dot{m} = \rho u A = GA. \tag{A3}$$

The total mass flow rate in the pipe is also expressed as the integral of the local mass flux (ρu) over the cross section

$$\dot{m} = \int_A (\rho u)\, dA. \tag{A4}$$

Hence

$$u = \frac{\int_A (\rho u)\, dA}{\rho A} = \frac{2\pi\rho}{\rho\pi a^2} \int_0^a u\,(r,z)\, r\, dr = \frac{2}{a^2} \int_0^a u\,(r,z)\, r\, dr. \tag{A5}$$

The last expression corresponds to the mean velocity for incompressible flow in a circular tube of radius a and hydraulic diameter $D = 2a$.

The mean temperature is defined so that the product $\dot{m} C_p T$ is equal to the true rate of thermal energy advection integrated over the cross section. This true advection rate is given by integrating the product of the local mass flux (ρu) and the local thermal energy per unit mass ($C_p T$), over the cross section A of the duct

$$T = \frac{\int_A (\rho u)\,(C_p T)\, dA}{\rho u C_p A}. \tag{A6}$$

For flow in a circular tube with constant ρ and C_p it follows that

$$T = \frac{2}{u a^2} \int_0^a u\,(r,z)\, T\,(r,z)\, r\, dr. \tag{A7}$$

The transverse (radial) heat transfer into the pipe is given by Newton's law of cooling

$$q = h\,(T_s - T)\,, \tag{A8}$$

where q, the convective heat flux in $\mathrm{W\,m^{-2}}$, is proportional to the difference between the surface and mean fluid temperatures, T_s and T, respectively. The value of T must vary in the flow direction z if heat transfer is occurring, that is, dT/dz is never zero along the pipe. The convection heat transfer coefficient, or film resistance h, is usually calculated from empirical correlations.

For fully developed (hydrodynamically and thermaly) turbulent flow in a smooth pipe, the local Nusselt number may be obtained from the Dittus-Boelter correlation [9] for heating the fluid

$$\mathrm{Nu} = 0.023 \mathrm{Re}^{4/5} \mathrm{Pr}^{2/5}. \tag{A9}$$

The range of validity is $0.6 \leq \mathrm{Pr} \leq 160$, $\mathrm{Re} \geq 10^4$ and $L \geq 10D$, where L is the length of the pipe. This equation is valid for smooth pipes and recommended only for moderate temperature differences between the fluid and the pipe wall. All the properties are evaluated at the mean fluid temperature. Simplifying eq. (A9) the convection heat transfer coefficient can be written as

$$h = 0.023 \rho^{4/5} k^{3/5} \left(\frac{C_p}{\mu}\right)^{2/5} \frac{u^{4/5}}{D^{1/5}}. \tag{A10}$$

Using the thermophysical properties of water listed in Appendix B, a first order expansion in T gives

$$h \cong 1.44 \times 10^3\,(1 + 0.015T)\, \frac{u^{4/5}}{D^{1/5}}, \tag{A11}$$

which is used in Ref. [15] for the design of solenoid magnets. Figure (10) shows a plot of the heat transfer coefficient according to the Dittus-Boelter correlation versus the mean temperature of the fluid.

The Dittus-Boelter correlation may lead to errors as large as 25%. More recent correlations may reduce such errors to less than 10%. The Gnielinski correlation [13] applies for either uniform surface heat flux or uniform surface temperature

$$\mathrm{Nu} = \frac{(f_D/8)\,(\mathrm{Re} - 1000)\,\mathrm{Pr}}{1 + 12.7\,(f_D/8)^{1/2}\left(\mathrm{Pr}^{2/3} - 1\right)}, \tag{A12}$$

where f_D is the Darcy friction factor (H. Darcy introduced the concept of the pipe roughness scaled by the diameter in 1857). The correlation (A12) is valid for $0.5 \leq \mathrm{Pr} \leq 2000$ and $3000 \leq \mathrm{Re} \leq 5 \times 10^6$

and all properties should be evaluated at the mean fluid temperature T. The friction factor f_D for fully developed laminar flow and Re$\leq$ 2300 is

$$f_D = \frac{64}{\mathrm{Re}}. \tag{A13}$$

For fully developed turbulent flow and Re$\geq 4 \times 10^3$ the friction factor is described by the Colebrook formula [10]

$$\frac{1}{\sqrt{f_D}} = -2\log_{10}\left(\frac{\varepsilon/D}{3.70} + \frac{2.51}{\mathrm{Re}\sqrt{f_D}}\right), \tag{A14}$$

where ε is the surface roughness. The friction factor can be expressed in terms of the Reynolds number and the surface roughness using the principal value of the Lambert function W, which is the inverse function of $f(W) = W\exp W$

$$f_D = \begin{cases} \dfrac{64}{\mathrm{Re}} & (\mathrm{Re} \leq 2300) \\ \left[\dfrac{\mathrm{Re}}{2.51}\dfrac{\varepsilon/D}{3.70} - \dfrac{2}{\ln 10}W\left(\dfrac{\ln 10}{2}\dfrac{\mathrm{Re}}{2.51}\sqrt{10^{\frac{\mathrm{Re}}{2.51}\frac{\varepsilon/D}{3.70}}}\right)\right]^{-2} & \left(\mathrm{Re} \geq 4\times 10^3\right) \end{cases}. \tag{A15}$$

The Moody diagram [11] shown in Fig. 11 is a plot of friction factor versus the Reynolds number, with the relative roughness ε/D as parameter. In the transition region 2300 $\leq$ Re$\leq 4\times 10^3$, where the flow may be either laminar or turbulent, the correlation for fully turbulent conditions overpredicts the convection heat transfer coefficient. The Churchill equation for the friction factor [14] provides a transition between the friction factor given by the Colebrook equation (A14) in the turbulent regime and the friction factor $f_D = 64/Re$ in the laminar regime:

$$\begin{aligned} f_D &= 8\left[\left(\frac{8}{\mathrm{Re}}\right)^{12} + \frac{1}{(A'+B')^{3/2}}\right]^{1/12}, \\ A' &= \left\{-2.457\ln\left[\left(\frac{7}{\mathrm{Re}}\right)^{9/10} + 0.27\frac{\varepsilon}{D}\right]\right\}^{16}, \\ B' &= \left(\frac{37530}{\mathrm{Re}}\right)^{16}. \end{aligned} \tag{A16}$$

The right picture in Fig. 11 shows a comparison of the friction factor calculated using equations (A13) and (A14), and using the Churchill eq. (A16). This equation applies to all three flow regimes – laminar, transitional, and turbulent.

Figure 12 shows the turbulent flow heat transfer coefficient versus the mean temperature of water calculated using the Gnielinski correlation (A12) with the friction factor given by the Churchill equation (A16). The figure also compares results obtained with the Dittus-Boelter equation (A9) and the laminar flow expression $h = (48/11)k/D$.

In single-phase convection the heat flux is linear with surface temperature as given by Newton's law of cooling. At the onset of boiling, when the surface temperature exceeds the saturation temperature, the heat flux becomes nonlinear with respect to surface temperature. In high heat flux applications large temperature gradients occur even without boiling. In these cases the variation of physical properties with temperature over the flow cross section affects the heat transfer before saturation. For liquids far from their critical point only dynamic viscosity varies greatly with temperature, and the heat transfer coefficient is modified by a property correction factor recommended by Petukhov [12], which introduces a slight nonlinearity with surface temperature. Introducing the Petukhov property correction factor in the Gnielinski correlation (A12), the convection heat transfer coefficient can be written as

$$h = \frac{k}{D}\frac{(f_D/8)(\mathrm{Re}-1000)\,\mathrm{Pr}}{1+12.7\,(f_D/8)^{1/2}\left(\mathrm{Pr}^{2/3}-1\right)}\left(\frac{\mu}{\mu_s}\right)^{0.11}, \tag{A17}$$

where μ and μ_s are the values of the dynamic viscosity calculated at the mean fluid temperature T and surface temperature T_s, respectively. The mean temperature T is used for all other fluid properties. The Darcy friction factor f_D is calculated using the Churchill eq. (A16).

The heat transfer for internal flows can be enhanced by increasing the convection coefficient and/or the convection surface area. This can be achieved introducing coiled wire or twisted tape inserts in the tube,

or machining helical grooves or longitudinal fins in the inner surface of the tube. The inserts or helical grooves introduce a tangential velocity component which increases the speed of the flow, particularly in laminar flow conditions and near the tube wall. However, in the turbulent flow regime the heat coefficient is effectively increased by introducing surface roughness, as indicated in Figs. 11 and 12. Of course, this increases the pressure drop and related pump power requirement.

The pressure drop due to friction along a given length of pipe L and hydraulic diameter D is expressed by the phenomenological Darcy-Weisbach equation (written in the present form by J. Weisbach in 1845)

$$\Delta p = f_D \frac{L}{D} \frac{\rho u^2}{2} = f_D \frac{L}{D} \frac{G^2}{2\rho}. \tag{A18}$$

This equation refers to fully developed, steady-state and incompressible flow. Figure 13 shows the pressure drop versus the mean temperature of the fluid along a pipe of given length and hydraulic diameter calculated using eq. (A18). This figure refers to constant mass flux G showing the variation of the pressure drop due to the combined variation of friction factor (Reynolds number) and density with temperature, for fixed geometry of the pipe.

Appendix B: Thermophysical properties of water (liquid phase)

For high values of the toroidal magnetic field the center post cooling system may operate with water in the superheated regime, between the usual boiling point $100°C$ and near the critical temperature $\sim 374°C$. The correlations presented in this Appendix are fitted to tables for the thermophysical properties of saturated water obtained from the National Institute of Standards and Technology (NIST) [22]. Excepting vapor pressure and viscosity the correlations are limited to the range $0°C \leq T \leq 360°C$ to avoid large order polynomial expansions and simplify the equations. In particular, the equations do not represent the singular behavior of the specific heat capacity and thermal conductivity near the critical point.

Vapor pressure ($0°C \leq T \leq 373.946°C$): The vapor pressure of water is approximated using an extended form of the Antoine equation

$$\begin{aligned} p\left(T\right) &= p_0 + \left(p_c - p_0\right)\left(\frac{T-T_0}{T_c-T_0}\right)\left[1 + a\left(\frac{T+T_c}{2T_c} - 1\right) + b\left(\frac{T+T_c}{2T_c} - 1\right)^2\right] \\ &\quad \exp\left[c\left(\frac{2T_c}{T+T_c} - 1\right) + d\left(\frac{T-T_c}{T_c}\right) + e\left(\frac{T-T_c}{T_c}\right)^2 + f\left(\frac{T-T_c}{T_c}\right)^3\right], \end{aligned} \tag{B1}$$

where $p_0 = 611.213\,\mathrm{Pa}$ is the vapor pressure of water at $T_0 = 0°C$ and $p_c = 22.064\,\mathrm{MPa}$= $220.64\,\mathrm{bar}$ is the critical absolute pressure at the critical temperature $T_c = 373.946°C$. The fitting coefficients are $a = 4.05321$, $b = 10.1326$, $c = 23.5621$, $d = 13.2085$, $e = -6.38977$ and $f = 11.3147$. Figure 14 shows the comparison between the fitted eq. (B1) and NIST data.

Density ($0°C \leq T \leq 360°C$): The density of saturated water is approximated by the polynomial

$$\begin{aligned} \rho\left(T\right) &= \rho_0\left[1 + a\left(\frac{T-T_0}{T_c}\right)^2 + b\left(\frac{T-T_0}{T_c}\right)^3 + c\left(\frac{T-T_0}{T_c}\right)^4 + d\left(\frac{T-T_0}{T_c}\right)^5\right. \\ &\quad \left. + e\left(\frac{T-T_0}{T_c}\right)^6 + f\left(\frac{T-T_0}{T_c}\right)^7 + g\left(\frac{T-T_0}{T_c}\right)^8\right], \end{aligned} \tag{B2}$$

where $T_0 = 4°C$ and $\rho_0 = 999.925\,\mathrm{kg\ m^{-3}}$. The critical density is $\rho_c = 322.00\,\mathrm{kg\ m^{-3}}$ at the critical temperature $T_c = 373.946°C$. The fitting coefficients are $a = -1.23266$, $b = 5.67161$, $c = -23.4734$, $d = 58.8874$, $e = -84.1951$, $f = 62.9222$ and $g = -19.1647$. Figure 15 shows the comparison between the fitted eq. (B2) and NIST data.

Specific heat capacity ($0°C \leq T \leq 360°C$): The specific heat capacity of saturated water is approximated by the rational function

$$C_p\left(T\right) = \frac{a + bT + cT^2 + dT^3 + eT^4 + fT^5 + gT^6}{1 + hT + iT^2}. \tag{B3}$$

The fitting coefficients are $a = 4220.33$, $b = 231.097$, $c = -0.639883$, $d = 0.000113674$, $e = 7.15687 \times 10^{-7}$, $f = -1.25293 \times 10^{-9}$, $g = -1.41173 \times 10^{-12}$, $h = 0.0557337$ and $i = -0.000156793$. Figure 16 shows the comparison between the fitted eq. (B3) and NIST data.

Dynamic viscosity ($0°C \leq T \leq 373.946°C$): The dynamic viscosity of saturated water is approximated by the rational function

$$\mu(T) = \frac{\mu_0}{1 + a(T - T_0) + b(T - T_0)^2 + c(T - T_0)^3 + d(T - T_0)^4}, \tag{B4}$$

where $\mu_0 = 1002.0 \times 10^{-6}$ Pa s is the standard viscosity of water at $T_0 = 20°C$. The fitting coefficients are $a = 0.0247453$, $b = 0.000126083$, $c = -5.57223 \times 10^{-7}$ and $d = 1.06282 \times 10^{-9}$. Figure 17 shows the comparison between the fitted eq. (B4) and NIST data.

Thermal conductivity ($0°C \leq T \leq 360°C$): The thermal conductivity of saturated water is approximated by the polynomial

$$k(T) = a + bT + cT^2 + dT^3 + eT^4. \tag{B5}$$

The fitting coefficients are $a = 0.560941$, $b = 0.00216031$, $c = -0.0000119445$, $d = 2.47066 \times 10^{-8}$ and $e = -3.11265 \times 10^{-11}$. Figure 18 shows the comparison between the fitted eq. (B5) and NIST data.

Prandtl ($0°C \leq T \leq 360°C$): The Prandtl number is defined by

$$\Pr(T) = \frac{C_p(T)\,\mu(T)}{k(T)}. \tag{B6}$$

Figure 19 shows a comparison between the Prandtl's number given by eq. (B6) and data points obtained from reference [23].

Saturation temperature ($0.00061165\,\text{MPa} \leq p \leq 22.064\,\text{MPa}$): The temperature of saturated water as a function of pressure is approximated by a modified form of the Antoine equation

$$T_{\text{sat}}(p) = T_0 + (T_0 - T_c)\left(1 - \frac{1}{\ln\left[(p_c/p_0)^{\alpha}\right]}\right)\left(\frac{1}{1 - \ln\left[(p/p_0)^{\alpha}\right]} - 1\right), \tag{B7}$$

where the vapor pressure of water at $T_0 = 0°C$ is $p_0 = 611.213$ Pa and the critical pressure is $p_c = 22.064\,\text{MPa} = 220.64\,\text{bar}$ at the critical temperature $T_c = 373.946°C$. The fitting coefficient is $\alpha = 0.0581069$. Figure 20 shows the comparison between the fitted eq. (B7) and NIST data. Using the value of pressure $p = 0.101325\,\text{MPa}$ corresponding to the normal boiling point of water $T = 99.9743°C$ gives $\alpha = 0.0586639$. The standard IUPAC boiling point of water $p = 0.1\,\text{MPa}$, $T = 99.61°C$ gives $\alpha = 0.0586624$.

Appendix C: Center post cooling channels configuration

The present study was carried out for a simplified configuration of the central column, consisting of wedged trapezoidal sectors formed by trapezoidal or rectangular copper bars separated by copper rods. Figure 21 shows diverse configurations for the TF coil central column. The simplest configuration consists of a cylindrical post with cooling holes drilled along the length of the column. This is the most efficient configuration for cooling purposes, but of difficult fabrication in a long-length column. Alternatively, the hollow copper bars may be fabricated by extrusion, but care must be taken to obtain the final hard-tempered product. The TF coil of constant rectangular or square cross-sections also shown in Fig. 21 could be fabricated as single pieces using stacked circular cables, or hollow conductors. These cables would by under pure tension with only one interruption at the electrical leads. Unfortunately, these constant cross-section coils do not make full use of the center post space, which is at a premium in compact configurations.

Acknowledgment: This work was supported by a grant provided by the *Programa de Capacitação Institucional: Diretoria de Pesquisa e Desenvolvimento/Comissão Nacional de Energia Nuclear (CNEN).*

[1] R. D. Stambaugh, V.S. Chan, R.L. Miller and M.J. Schaffer. 1998 "The spherical tokamak path to fusion power" *Fusion Technol.* **33**, 1-12

[2] K. Tobita, S. Nishio, M. Sato, S. Sakurai, T. Hayashi, Y.K. Shibama, T. Isono, M. Enoeda, H. Nakamura, S. Sato, K. Ezato, T. Hayashi, T. Hirose, S. Ide, T. Inoue, Y. Kamada, Y. Kawamura, H. Kawashima, N. Koizumi, G. Kurita, Y. Nakamura, K. Mouri, T. Nishitani, J. Ohmori, N. Oyama, K. Sakamoto, S. Suzuki, T. Suzuki, H. Tanigawa, K. Tsuchiya and D. Tsuru. 2007 "SlimCS – compact low aspect ratio DEMO reactor with reduced-size central solenoid" *Nucl. Fusion* **47**, 892-899

[3] G.M. Voss, S. Davis, A. Dnestrovskij, A. Kirk, P.J. Knight, M. Loughlin, M.H. O'Brien, D. Sychugov, A. Tabasso, H.R. Wilson. 2008 "Conceptual design of a component test facility based on the spherical tokamak" *Fusion Eng. Des.* **83**, 1648-1653

[4] G.O. Ludwig, M.C.R. Andrade, M. Gryaznevich and T.N. Todd. 2009 "Physics performance analysis of low-power tokamak reactors" *Nucl. Fusion* **49**, 085026-20pp

[5] M. Kotschenreuther, P. Valanju, S. Mahajan, L.J. Zheng, L.D. Pearlstein, R.H. Bulmer, J. Canik and R. Maingi. 2010 "The super X divertor (SDX) and a compact fusion neutron source (CFNS)" *Nucl. Fusion* **50**, 035003-8pp

[6] B.V. Kuteev, E.A. Azizov, A.S. Bykov, A.Yu. Dnestrovsky, V.N. Dokuka, G.G. Gladush, A.A. Golikov, P.R. Goncharov, M. Gryaznevich, M.I. Gurevich, A.A. Ivanov, R.R. Khairutdinov, V.I. Khripunov, D. Kingham, A.V. Klishchenko, V.A. Kurnaev, V.E. Lukash, S.Yu. Medvedev, P.V. Savrukhin, V.Yu. Sergeev, Yu.S. Shpansky, A. Sykes, G. Voss and A.V. Zhirkin. 2011 "Steady-state operation in compact tokamaks with copper coils" *Nucl. Fusion* **51**, 073013-6pp

[7] K. Gi, Y. Ono, M. Nakamura, Y. Someya, H. Utoh, K. Tobita and M. Ono. 2015 "Conceptual design study of the moderate size superconducting spherical tokamak power plant" *Nucl. Fusion* **55**, 063036-14pp

[8] B.N. Sorbom, J. Ball, T.R. Palmer, F.J. Mangiarotti, J.M. Sierchio, P. Bonoli, C. Kasten, D.A. Sutherland, H.S. Barnard, C.B. Haakonsen, J. Goh, C. Sung, and D.G. Whyte. 2015 "ARC: A compact, high-field, fusion nuclear science facility and demonstration power plant with demountable magnets" *Fusion Eng. Des.* **100**, 378-405

Articles on turbulent heat transfer: in cronological order

[9] E.J. Dittus and L.M.K. Boelter. 1930 "Heat transfer in automobile radiators of tubular type", Univ. California Berkeley, *Publications on Engineering* **2**, 443-461

[10] C.F. Colebrook. 1939 "Turbulent flow in pipes, with particular reference to the transition region between the smooth and rough pipe laws" *J. Inst. Civil Eng.* **11**, 133-156

[11] L.F. Moody. 1944 "Friction factors for pipe flow" *Trans. ASME* **66**, 671-684

[12] B.S. Petukhov. 1970 "Heat transfer and friction in turbulent pipe flow with variable physical properties", In: *Advances in Heat Transfer*, Volume **6**, 503-564, Eds.: J.P. Hartnett and T.F. Irvine, Academic Press, New York, NY, USA

[13] V. Gnielinski. 1976 "New equation for heat and mass transfer in turbulent pipe and channel flow" *Int. Chem. Eng.* **16**, 359-368

[14] S.W. Churchill. 1977 "Friction factor equation spans all fluid-flow regimes" *Chem. Eng.* **7**, 91-92

Texts on magnet design and heat transfer:

[15] D.B. Montgomery. 1969 *Solenoid magnet design*, Wiley Interscience, New York, NY, USA

[16] R.J. Thome and J.M. Tarrh. 1982 *MHD and fusion magnets*, John Wiley and Sons, New York, NY, USA

[17] W.M. Rohsenow, J.P. Hartnett and Y.I. Cho (editors). 1998 *Handbook of Heat Transfer*, Third Edition, McGraw-Hill, New York, NY, USA

[18] J.H. Lienhard IV and J.H. Lienhard V. 2002 *A heat transfer textbook*, Third Edition, Phlogiston Press, Cambridge, Massachusetts, USA

[19] T.L. Bergman, A.S. Lavine, F.P. Incropera and D.P. Dewitt. 2011 *Fundamentals of heat and mass transfer*, Seventh Edition, John Wiley and Sons, Hoboken, NJ, USA

References on termophysical properties of water:

[20] J. Kestin , M. Sokolov and W.A. Wakeham 1978 "Viscosity of liquid water in the range $-8°C$ to $150°C$" *J. Phys. Chem. Ref. Data* **7** 941-948.

[21] M.L.V. Ramires, C.A. Nieto de Castro, Y. Nagasaka, A. Nagashima, M.J. Assael and W.A. Wakeham 1995 "Standard reference data for the thermal conductivity of water" *J. Phys. Chem. Ref. Data* **24** 1377-1381.

[22] 2014 *Thermophysical Properties of Fluid Systems in the NIST (National Institute of Standards and Technology) Chemistry WebBook*: webbook.nist.gov/chemistry/fluid.

[23] 2014 *Thermal Properties of Water in the Engineering Toolbox*: www.engineeringtoolbox.com/water-thermal-properties-d_162.html.

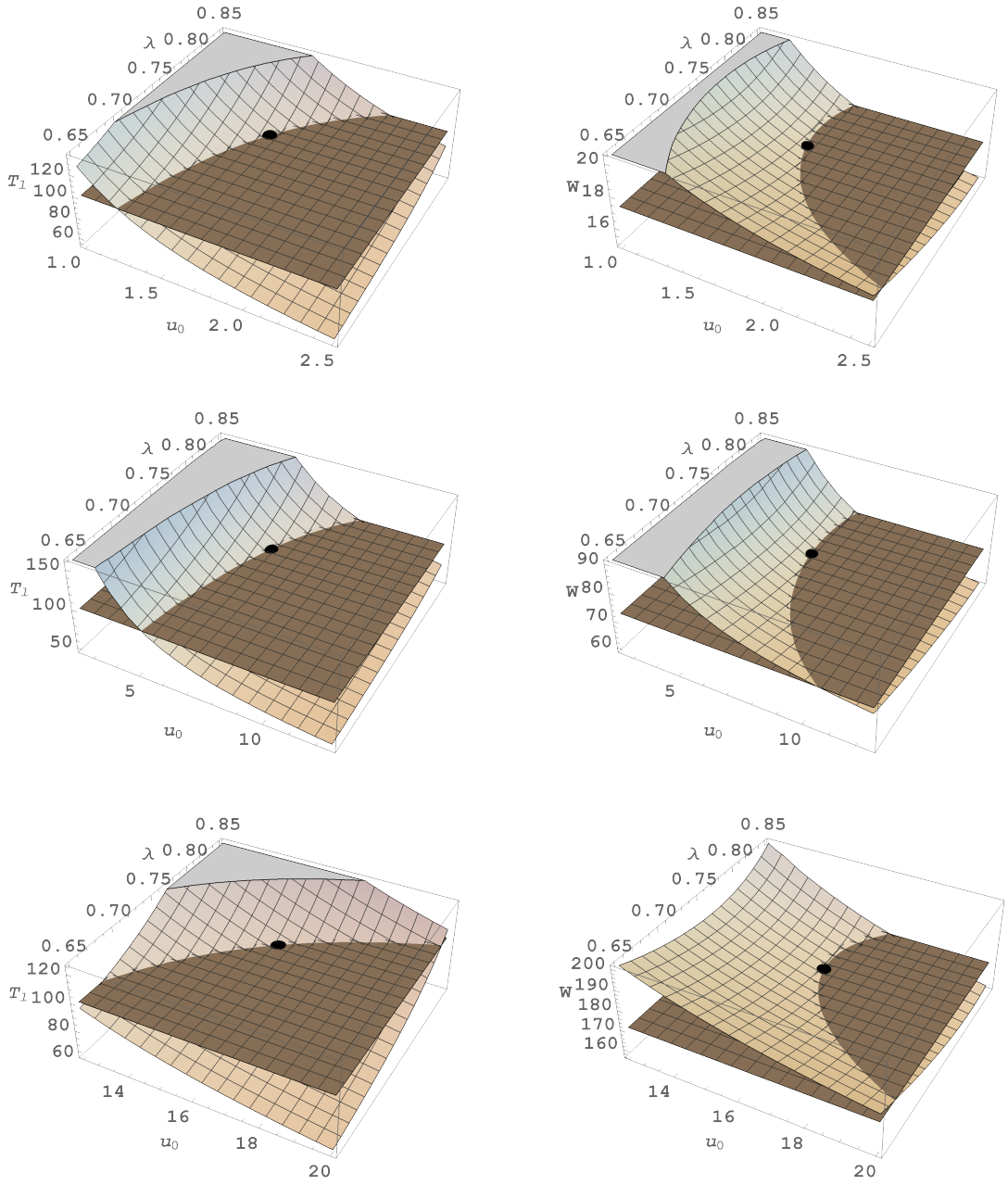

FIG. 5. The first and the second columns show the output average fluid temperature T_l and the dissipated power W, respectively, as functions of the input flow velocity u_0 and the copper fraction λ in smooth pipes (absolute roughness $\varepsilon = 0$). The horizontal planes correspond, in the first column, to the constant temperature $T_l = 100\,^{\circ}\mathrm{C}$ at the cooling channels output and, in the second column, to the power W dissipated in the output of the TF coil. The rows correspond, from top to bottom, to the values $B_0 = 1.0, 2.0$ and $3.0\,\mathrm{T}$ of the magnetic field. The central black points indicate the operating points, which correspond to the input flow velocity compatible with an output fluid temperature $T_l = 100\,^{\circ}\mathrm{C}$ and $\lambda = 0.780$. The parameters corresponding to these operating points are listed in Table I. Note the change of the scale in the flow velocity u_0 in m/s and in the power W in MW.

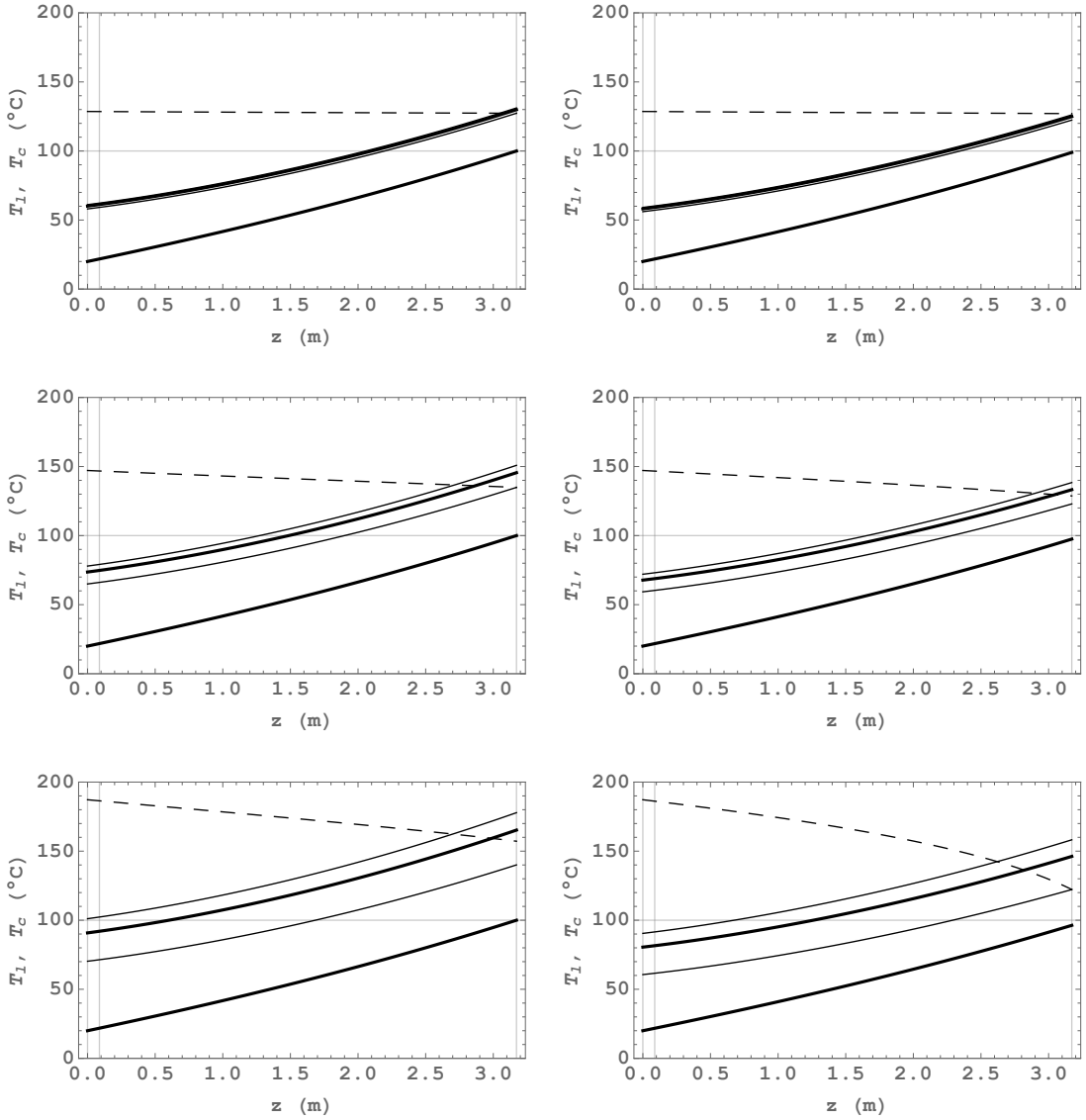

FIG. 6. Fluid, T_l, and conductor, T_c, average temperatures change along the cooling channels. The rows correspond, from top to bottom, to the values $B_0 = 1.0, 2.0$ and $3.0\,\mathrm{T}$ of the magnetic field. In each picture, the average fluid temperature is represented by the thick lower line. The thick upper line corresponds to the average conductor temperature, bounded by the surface, T_s (lower thin line), and maximum, $T_{\max}$ (upper thin line), temperatures of the conductor. The first column in the figure corresponds to smooth pipes with $\varepsilon = 0$, and the second column to rough pipes with $\varepsilon = 10\,\mu\mathrm{m}$. The thin vertical lines indicate the entrance region $0 < z < 10D$, where the thermal condition is not fully developed. The input flow velocity u_0 is adjusted, in each case, so that $T_l = 100\,^\circ\mathrm{C}$ at the end of the smooth pipes. The thin horizontal line indicates the usual boiling point $100\,^\circ\mathrm{C}$ at atmospheric pressure, and the thin dashed line the saturation temperature T_{sat} for a given input pressure p_0 and consistent pressure drop along the channels. The input pressure is adjusted, in each case, so that $T_s \leq T_{\mathrm{sat}}$ at the end of the cooling channels, either for smooth or rough pipes depending on the pressure drop conditions.

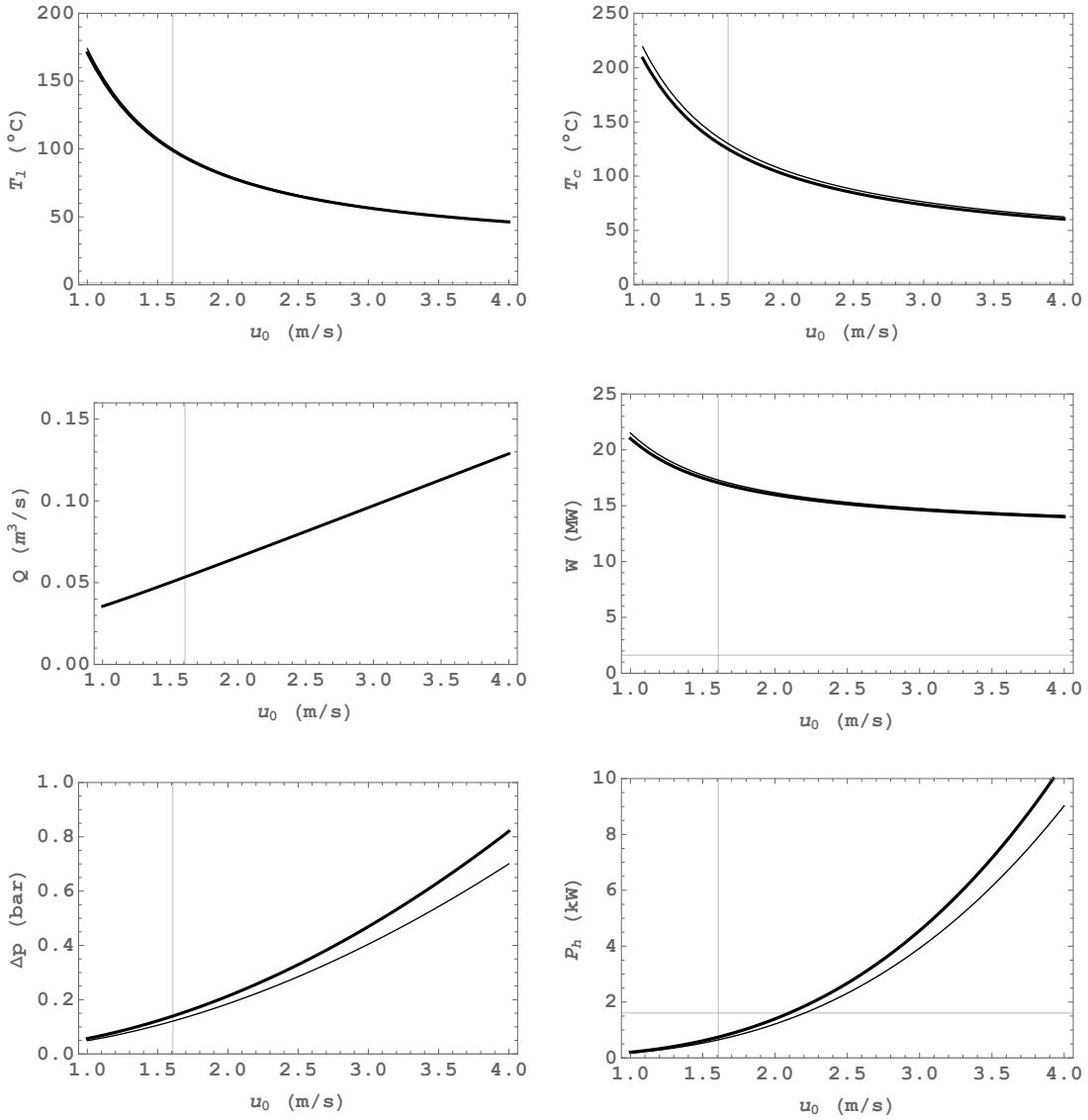

FIG. 7. Performance of the TF coil cooling system for $B_0 = 1.0\,\mathrm{T}$ as a function of the input flow velocity u_0. The sequence of pictures show: the average fluid temperature T_l, the average conductor temperature T_c, the total discharge Q, the total dissipated power W, the total pressure loss Δp, and the total pumping power P_h, for smooth, $\varepsilon = 0$ (thin lines), and rough, $\varepsilon = 10\,\mu\mathrm{m}$ (thick lines) cooling channels. The copper fraction is $\lambda = 0.780$. The thin vertical lines indicate the operating point $u_0 = 1.608\,\mathrm{m/s}$ listed in Table I.

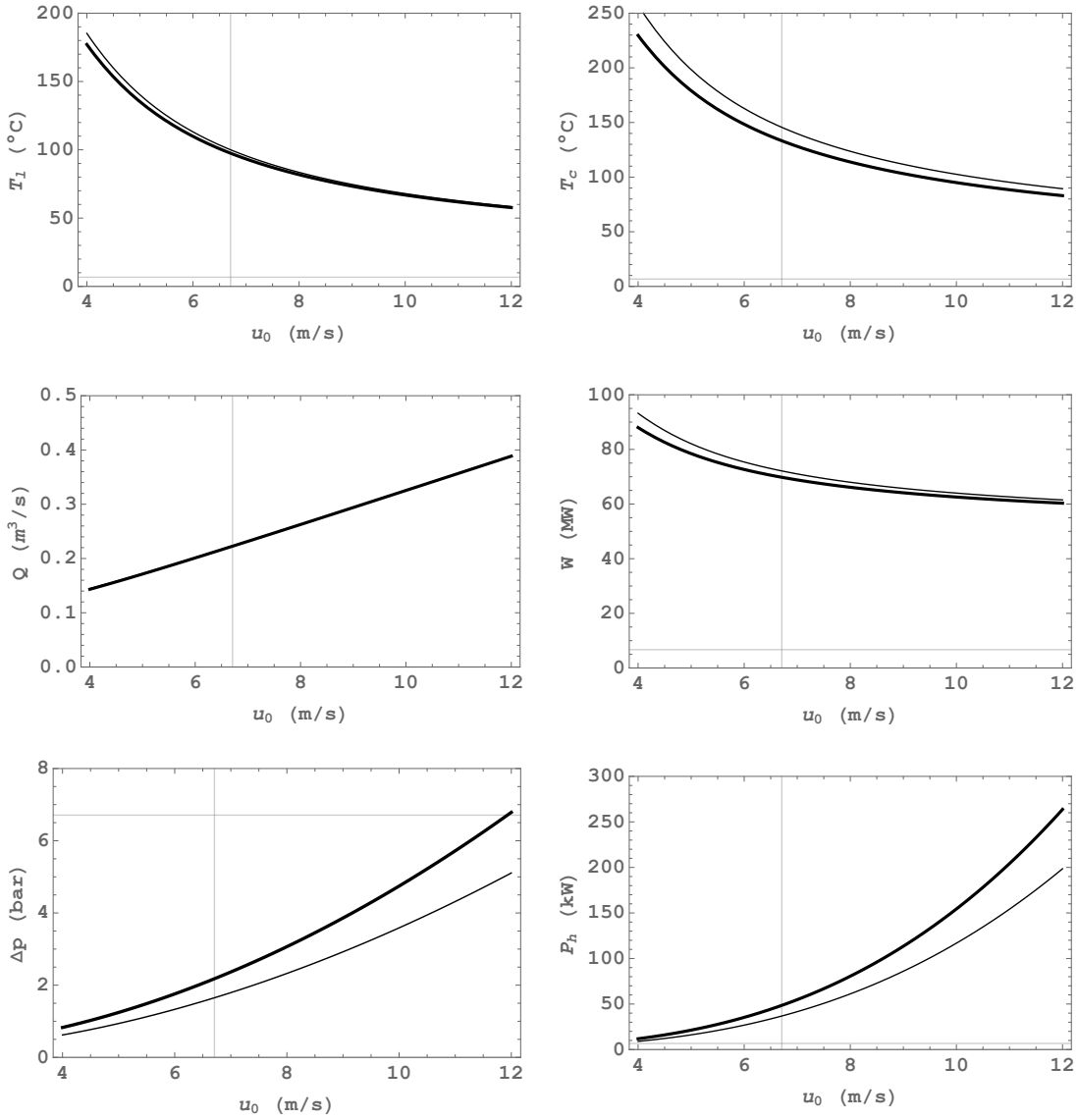

FIG. 8. Performance of the TF coil cooling system for $B_0 = 2.0\,\mathrm{T}$ as a function of the input flow velocity u_0. The sequence of pictures show: the average fluid temperature T_l, the average conductor temperature T_c, the total discharge Q, the total dissipated power W, the total pressure loss Δp, and the total pumping power P_h, for smooth, $\varepsilon = 0$ (thin lines), and rough, $\varepsilon = 10\,\mu$m (thick lines) cooling channels. The copper fraction is $\lambda = 0.780$. The thin vertical lines indicate the operating point $u_0 = 6.709\,\mathrm{m/s}$ listed in Table I.

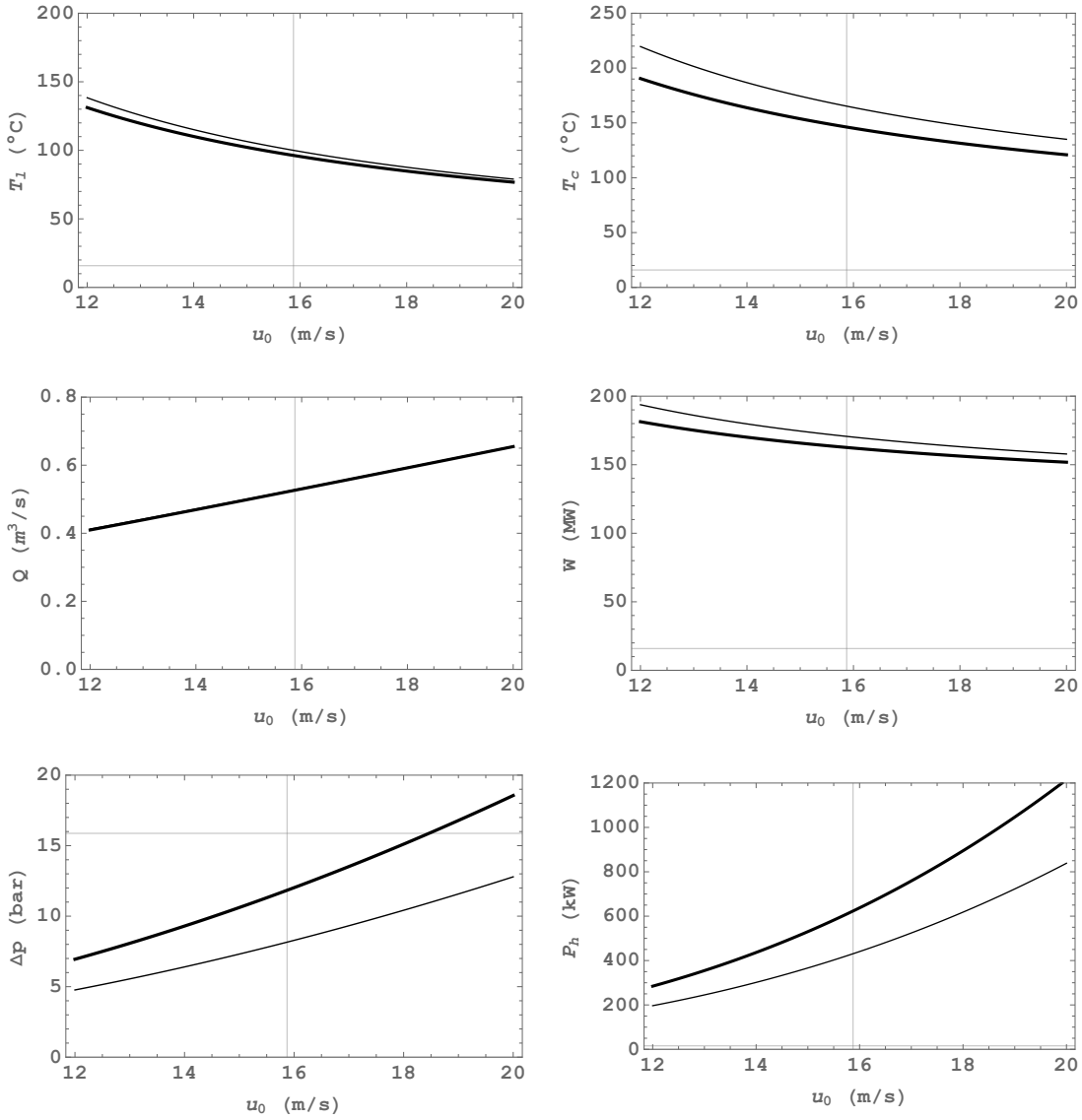

FIG. 9. Performance of the TF coil cooling system for $B_0 = 3.0\,\mathrm{T}$ as a function of the input flow velocity u_0. The sequence of pictures show: the average fluid temperature T_l, the average conductor temperature T_c, the total discharge Q, the total dissipated power W, the total pressure loss Δp, and the total pumping power P_h, for smooth, $\varepsilon = 0$ (thin lines), and rough, $\varepsilon = 10\,\mu$m (thick lines) cooling channels. The copper fraction is $\lambda = 0.780$. The thin vertical lines indicate the operating point $u_0 = 15.87\,\mathrm{m/s}$ listed in Table I.

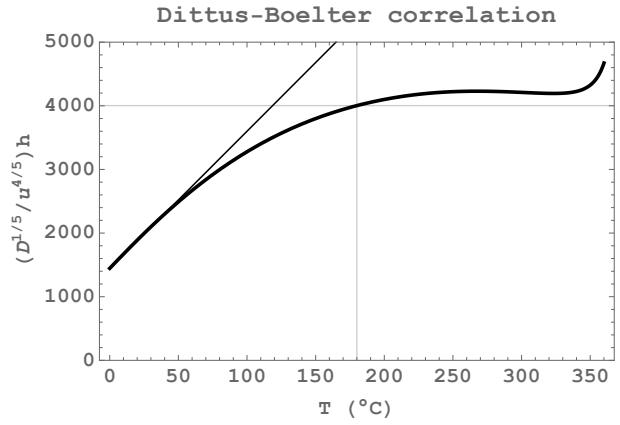

FIG. 10. Graphics of the heat transfer coefficient according to the Dittus-Boelter correlation (A10) – thick line – and the first-order expansion (A11) – thin line – versus the mean temperature of the fluid.

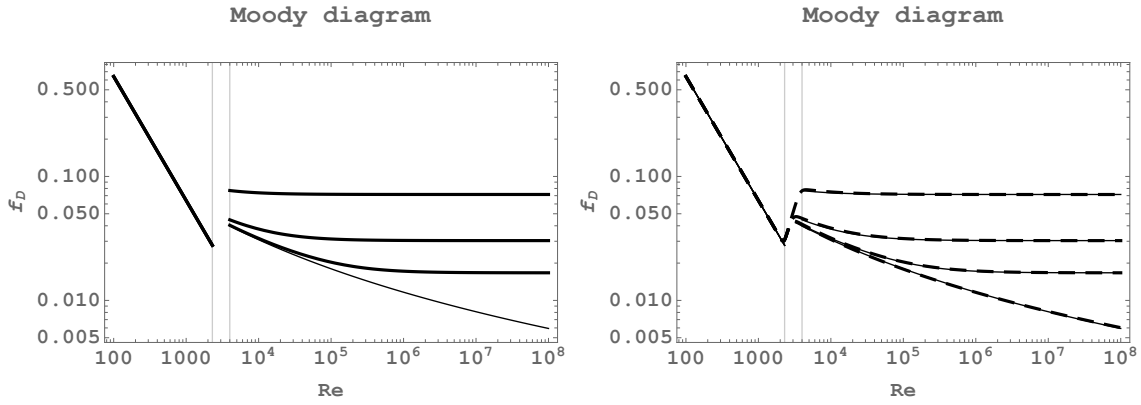

FIG. 11. Friction factor for fully developed flow in a pipe. Left picture: Plot of equations (A13) and (A14). The curves in the turbulent region $\mathrm{Re} \geq 4 \times 10^3$ correspond, from bottom to top, to values of the relative roughness $\varepsilon/D = 0$ (smooth pipe), 5×10^{-4}, 5×10^{-3}, and 5×10^{-2}, respectively. Right picture: Comparison of the friction factor calculated using equations (A13) and (A14) (continuous lines), and using the Churchill eq. (A16) (dashed lines).

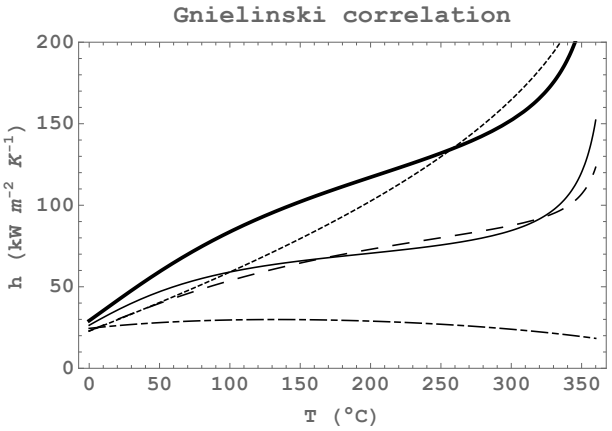

FIG. 12. Heat transfer coefficient as a function of the mean water temperature using the Gnielinski correlation (A12) for fully developed turbulent flow. The hydraulic diameter is $D = 1\,\mathrm{cm}$ and the mass flux is $G = 10^4\,\mathrm{kg\ m^{-2}\ s^{-1}}$ corresponding to a flow velocity $u \cong 10\,\mathrm{m\ s^{-1}}$ at $T = 4°C$ (maximum density of water). The solid thin line corresponds to a smooth pipe with absolute roughness $\varepsilon = 0$ and the solid thick line to a pipe with relative roughness $\varepsilon/D = 0.001$. The dashed thin line corresponds to the Dittus-Boelter equation (A9) and the dotted thin line to its first-order approximation (A11). The thin dot-dashed curve corresponds to 100 times the convective heat transfer coefficient for laminar flow, $h = (48/11)k/D$.

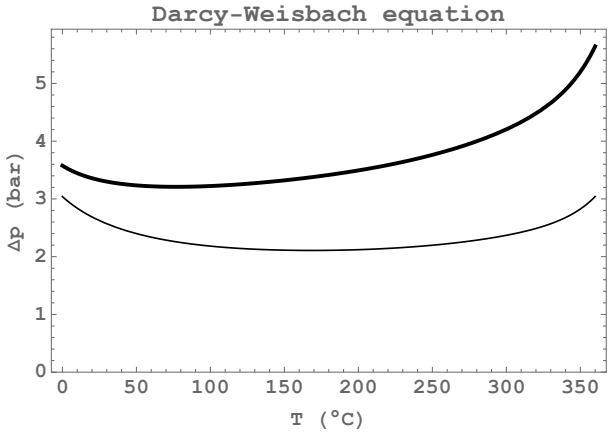

FIG. 13. Pressure drop as a function of the mean water temperature according to the Darcy-Weisbach eq. (A18). The pipe length is $L = 3\,\mathrm{m}$, the hydraulic diameter is $D = 1\,\mathrm{cm}$ and the mass flux is $G = 10^4\,\mathrm{kg\ m^{-2}\ s^{-1}}$ corresponding to a flow velocity $u \cong 10\,\mathrm{m\ s^{-1}}$ at $T = 4°C$. The solid thin line corresponds to a smooth pipe with absolute roughness $\varepsilon = 0$ and the solid thick line to a pipe with relative roughness $\varepsilon/D = 0.001$.

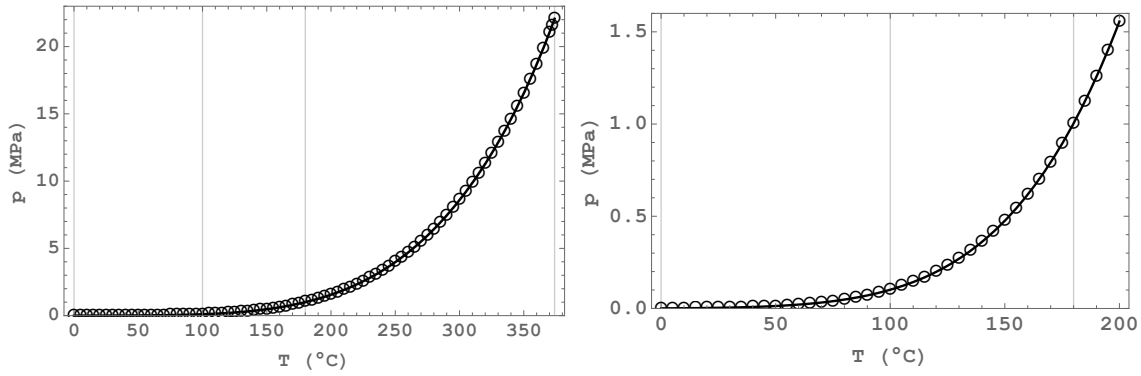

FIG. 14. Absolute pressure of saturated water. The thick line corresponds to the fitted eq. (B1) and the circles to NIST data points. The absolute pressure at $T \cong 100°C$ is 1.01420 bar. The figures show that the absolute pressure at $T \cong 180°C$ is $p = 10\,\mathrm{bar}$, which is about the maximum pressure level intended for usual cooling systems.

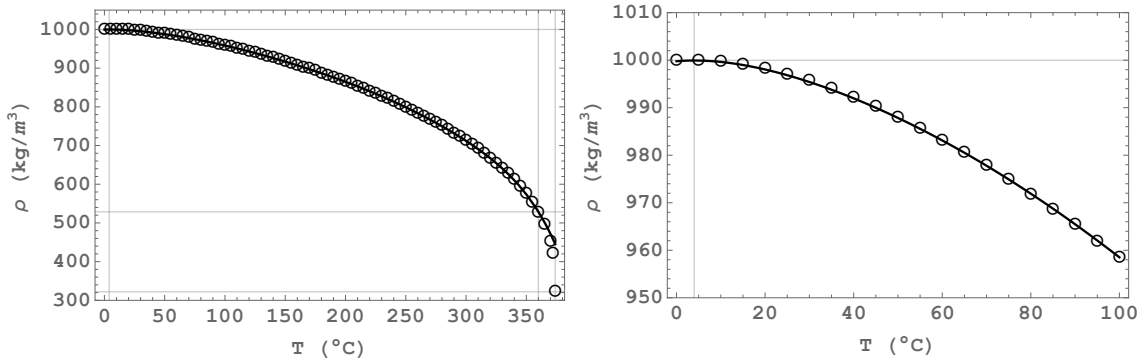

FIG. 15. Density of saturated water. The thick line corresponds to the fitted eq. (B2) and the circles to NIST data points. At ambient temperature the density of water takes the approximate constant value $\rho \cong 10^3\,\mathrm{kg\ m^{-3}}$. The maximum density of water is $999.9720\,\mathrm{kg\ m^{-3}}$ at $3.98°C$ and a pressure $p = 0.1\,\mathrm{MPa}$. The density of ice at $0°C$ is $916.8\,\mathrm{kg\ m^{-3}}$.

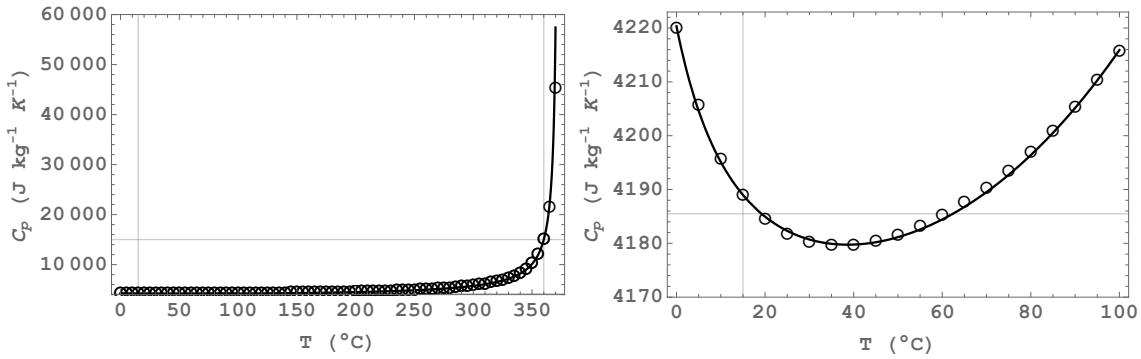

FIG. 16. Specific heat capacity of saturated water. The thick line corresponds to the fitted eq. (B3) and the circles to NIST data points. At ambient temperature the constant-pressure heat capacity of water takes the approximate constant value $C_p \cong 4186\,\mathrm{J\ kg^{-1}\ K^{-1}}$. The recommended value of the specific heat capacity of water at $15°C$ and a pressure $p = 0.1$ MPa is $4185.5\,\mathrm{J\ kg^{-1}\ K^{-1}}$. The specific heat capacity of ice at $-10°C$ is 2110 $\mathrm{J\ kg^{-1}\ K^{-1}}$ and at $0°C$ is $1960\,\mathrm{J\ kg^{-1}\ K^{-1}}$. The specific heat capacity of steam at $100°C$ is $2080\,\mathrm{J\ kg^{-1}\ K^{-1}}$.

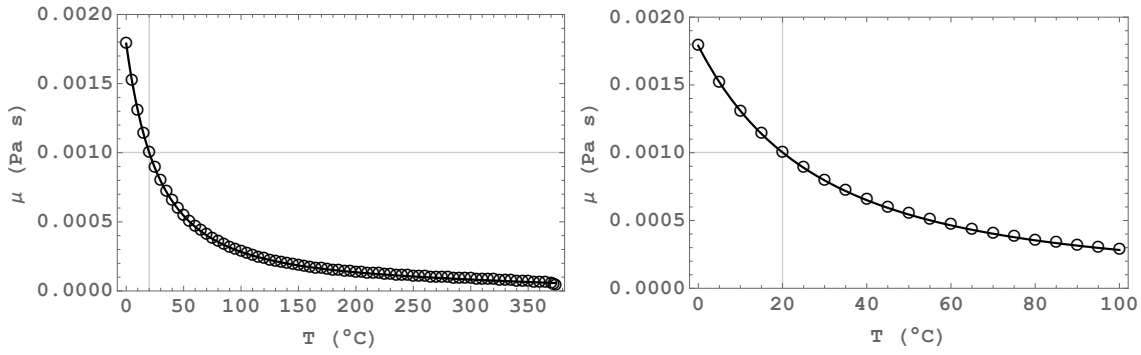

FIG. 17. Dynamic viscosity of saturated water. The thick line corresponds to the fitted eq. (B4) and the circles to NIST data points. The standard viscosity of water at $T_0 = 20°C$ is $\mu_0 = 1002.0 \times 10^{-6}\,\mathrm{Pa\ s}$.

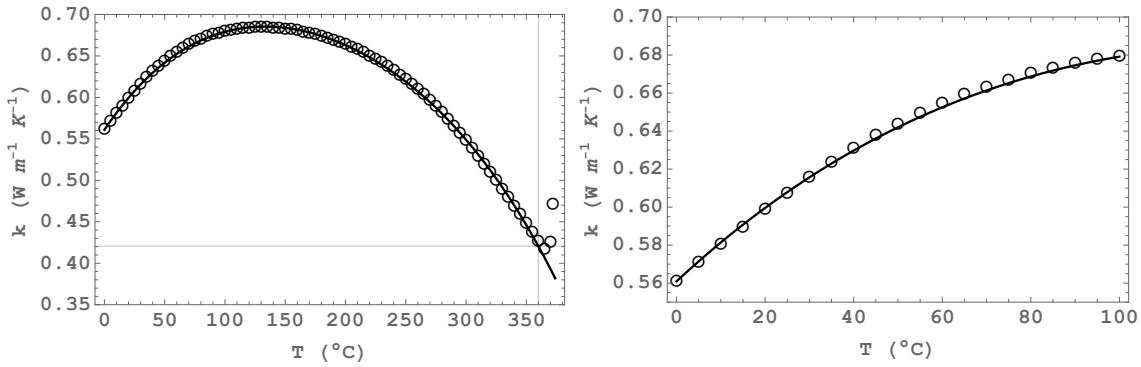

FIG. 18. Thermal conductivity of saturated water. The thick line corresponds to the fitted eq. (B5) and the circles to NIST data points. The standard thermal conductivity of water at the nominal temperature $T_0 = 25°C$ and a pressure $p = 1\,\text{bar}$ is $k_0 = 0.6065\,\text{W m}^{-1}\,\text{K}^{-1}$.

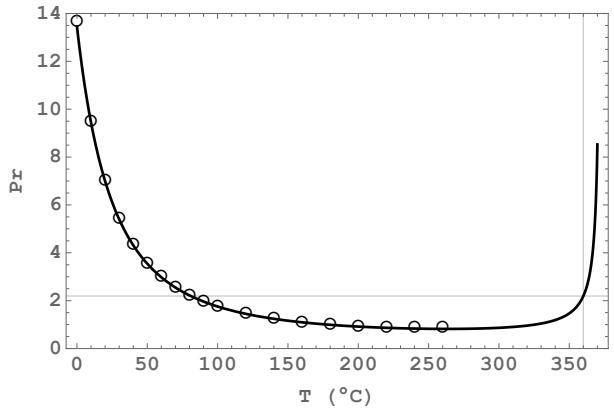

FIG. 19. Prandtl's number of saturated water. The thick line corresponds to eq. (B6) and the circles to data points obtained from reference[23].

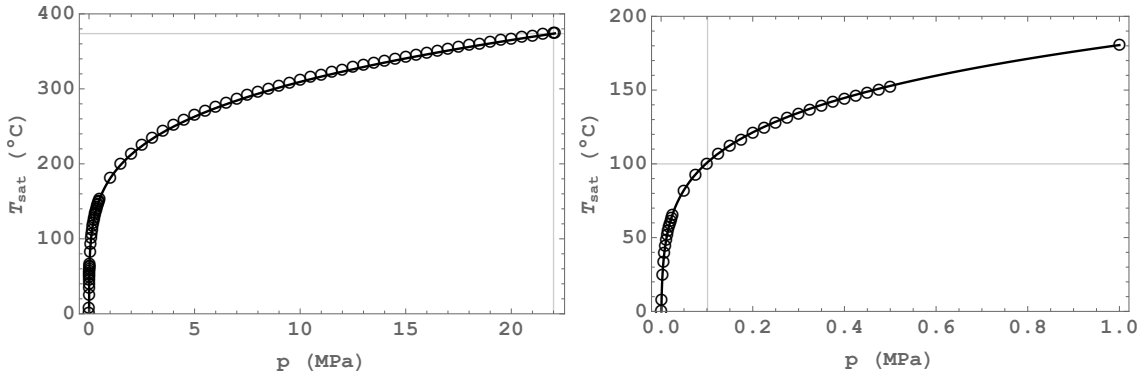

FIG. 20. Temperature of saturated water as a function of pressure (liquid phase). The thick line corresponds to the fitted eq. (B7) and the circles to NIST data points.

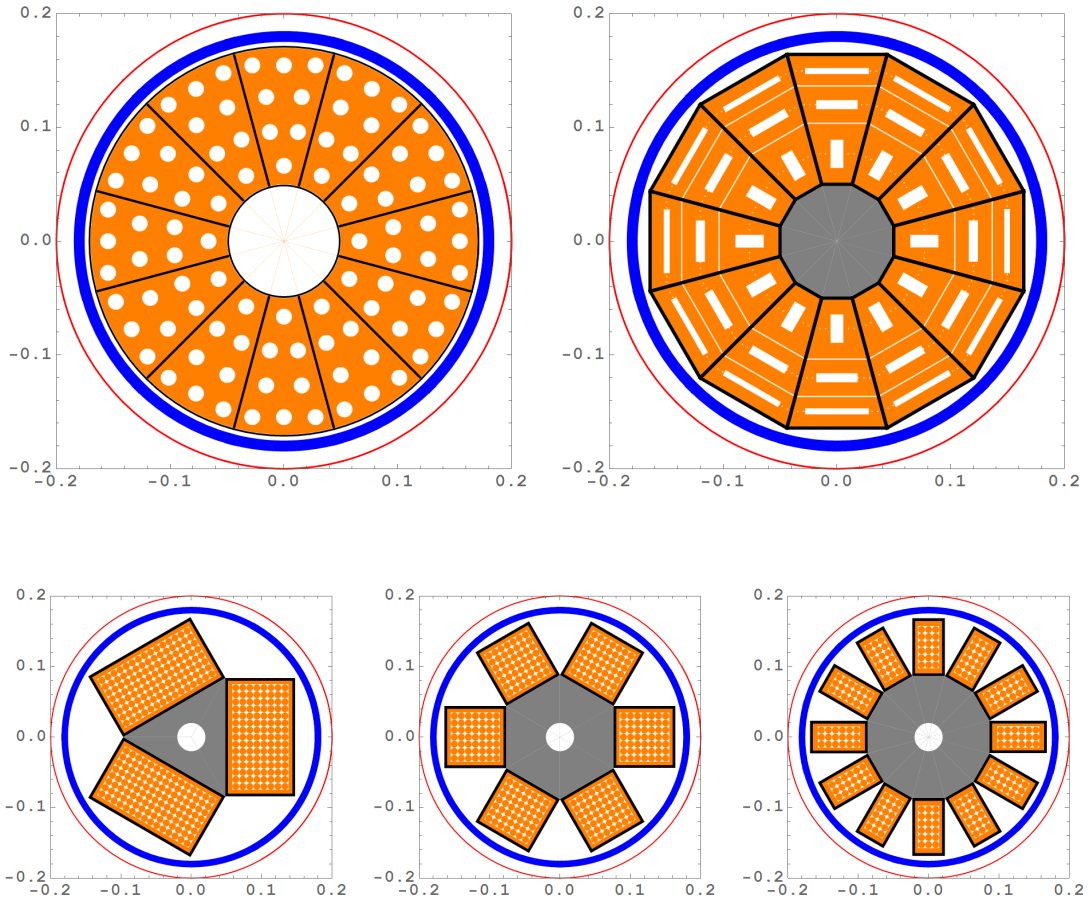

FIG. 21. The upper row shows, in the left hand side, a center post with drilled cooling holes and, in the right hand side, a central column formed by stacked, prefabricated bars. The lower row shows three examples of TF coil with rectangular or square cross-sections.